

RESEARCH

Open Access



Comparative transcriptomic analysis of perfluoroalkyl substances-induced responses of exponential and stationary phase *Escherichia coli*

Molly E. Wintenberg^{1*}, Olga B. Vasilyeva¹ and Samuel W. Schaffter¹

Abstract

Background Per- and polyfluoroalkyl substances (PFAS) are highly stable chemical contaminants of emerging concern for human and environmental health due to their non-natural chemistry, widespread use, and environmental persistence. Despite conventional metrology, mitigation strategies, and removal technologies, the complexity of this growing problem necessitates alternative approaches to tackle the immense challenges associated with complex environmental PFAS contamination. Recently, biology has emerged as an alternative approach to detect and mitigate PFAS and understand the molecular-level responses of living organisms to these compounds. However, little is understood of the impacts of PFAS on the environment, particularly impacts on microorganisms that play pivotal roles in nearly every ecosystem. Therefore, further study is needed to understand how microorganisms respond to different PFAS across growth phases.

Results In this study, we performed RNA sequencing at mid-exponential, early stationary phase, and late stationary phase of bacterial growth to determine the global transcriptional response of a model chassis, *Escherichia coli* MG1655, induced by two PFAS, perfluorooctanoic acid (PFOA) and perfluorododecanoic acid (PFDoA), and equivalent non-fluorinated carboxylic acids (NFCA), octanoic acid and dodecanoic acid. Differential gene expression analysis revealed PFOA and PFDoA induced distinct changes in gene expression throughout cultivation. Specifically, we identified significant changes in expression of the formate regulon and sulfate assimilation at mid-exponential phase and ferrous iron transport, central metabolism, the molecular chaperone network, and motility processes during stationary phase. Importantly, many of these changes were distinct from changes induced by NFCAs across growth phases.

Conclusions In summary, we find PFAS induce a system-level change in gene expression of metabolic, transport, and regulatory pathways, providing insight into how these non-natural chemicals interact with a model bacterium at various growth phases. In addition, the transcriptomic dataset presented could enable the development of future real-time environmental monitoring and mitigation technologies.

*Correspondence:
Molly E. Wintenberg
mwintenberg@gmail.com

Full list of author information is available at the end of the article



This is a U.S. Government work and not under copyright protection in the US; foreign copyright protection may apply 2025. **Open Access** This article is licensed under a Creative Commons Attribution 4.0 International License, which permits use, sharing, adaptation, distribution and reproduction in any medium or format, as long as you give appropriate credit to the original author(s) and the source, provide a link to the Creative Commons licence, and indicate if changes were made. The images or other third party material in this article are included in the article's Creative Commons licence, unless indicated otherwise in a credit line to the material. If material is not included in the article's Creative Commons licence and your intended use is not permitted by statutory regulation or exceeds the permitted use, you will need to obtain permission directly from the copyright holder. To view a copy of this licence, visit <http://creativecommons.org/licenses/by/4.0/>.

Keywords Transcriptomics, *Escherichia coli*, Per/polyfluoroalkyl substances, Differential gene expression, Exponential phase, Stationary phase

Introduction

Per- and polyfluoroalkyl substances (PFAS) are a class of fluorinated compounds with diverse structures conferring strong resistance to degradation or decomposition in the environment [1]. Widespread industrial production of fire-fighting foam and non-stick coatings and use in other consumer products of pesticides, cleaning materials, and personal care products, has led to substantial release of PFAS into the environment, raising concerns about their environmental persistence and bioaccumulation [2, 3]. PFAS have been detected ubiquitously in human hair, breast milk, and blood and in environmental populations, such as water basins, surface soils, and plants cultivated in contaminated sites [4–10]. Exposure to PFAS has been linked to several adverse human health effects, including immunotoxicity, liver damage, and thyroid dysfunction and negative ecological impacts of endocrine disruption in aquatic species [11–14].

To date, the U. S. Environmental Protection Agency (USEPA) and the international Organization of Economic Co-operation and Development (OECD) have categorized thousands of individual compounds based on a threshold of fluorine percentage and molecular structure or the presence of perfluoroalkyl moieties [15, 16]. The structures of these compounds are diverse with linear and branched carbon chains of varying length and fluorination and functional head groups containing sulfonates, sulfonamides, carboxylates, and other moieties that are believed to govern compound stability, transport, and environmental fate [17]. In addition to the variety of PFAS across industrial products, environmental samples from a single contaminated source will often contain mixtures of intact PFAS, partial degradation products, and precursor chemicals [18, 19]. Sample complexity and batch variation make measurement and quantitation of PFAS-containing samples with traditional analytical techniques like liquid chromatography – mass spectrometry (LC-MS) [20–22] challenging and costly. Moreover, water remediation strategies including ion exchange resins, high-pressure membrane systems, and granular activated carbon [23] and soil remediation strategies including thermal treatment and soil washing [24] are also complicated by the unique chemical properties that originally made PFAS efficient in industrial and commercial products. To rapidly respond to this growing problem, there is a need for alternative approaches to real-time environmental monitoring and mitigation efforts, as well as comprehensive methods to assess environmental impact [25–27]. Increasingly, researchers are turning to biology as an alternative approach for PFAS

detection [28, 29] and mitigation [25, 30]. Broad measurements of living systems could not only aid in rapid, on-site detection of new contamination sources and identification and classification of new PFAS byproducts but also expand our general understanding of the biological consequences of PFAS contamination [25, 26].

Bacteria are a promising measurement platform as they play critical roles in most ecosystems, are highly concentrated in soil environments and aquifers where PFAS contamination persists [31, 32], rapidly sense and respond to environmental fluctuations [33, 34], and have been reported to bioaccumulate PFAS [35]. Transcriptomic analysis by RNA sequencing (RNA-seq) of bacterial interactions with PFAS could serve as an alternative measurement strategy to explore genome-wide molecular mechanisms underlying gene expression level changes induced by PFAS. RNA-seq is a widely applicable technique that can investigate the response of a wide variety of organisms to various types and mixtures of PFAS, potentially enabling the identification of specific sensing gene targets and PFAS degradation pathways and provide insight into how these non-natural chemicals interact with living systems. Although, omics-based analyses have been used to examine the biological response of several organisms, including primary human liver cell spheroids, zebrafish, and *Escherichia coli*, to various PFAS [36–39], studies exploring the global transcriptional response of bacteria across key growth phases are limited.

In this study, we employed time course RNA-seq at key phases of bacterial growth to investigate the global transcriptional response of a model Gram-negative bacterium, *E. coli* MG1655, to PFAS (Fig. 1). *E. coli* is an optimal organism to begin understanding the microbial transcriptional responses to PFAS, as it is present in different environments and its transcriptional responses to numerous stressors and growth conditions have been extensively studied with RNA-seq [40–43]. *E. coli* was grown in the presence of perfluoroalkyl carboxylic acids (PFCA) or equivalent non-fluorinated carboxylic acids (NFCA) at a concentration of 100 $\mu\text{mol/L}$ for 48 h, and samples were sequenced at mid-exponential and stationary phase. Differential expression analysis revealed significant changes in mid-exponential and stationary phase gene expression induced by two different PFCAs, including changes that differed from the NFCAs. Our results indicate *E. coli* employed different mechanisms at different growth phases further signifying temporal gene expression in response to PFCAs. Specifically, we identified significant changes in the expression of the formate regulon and sulfate assimilation at mid-exponential

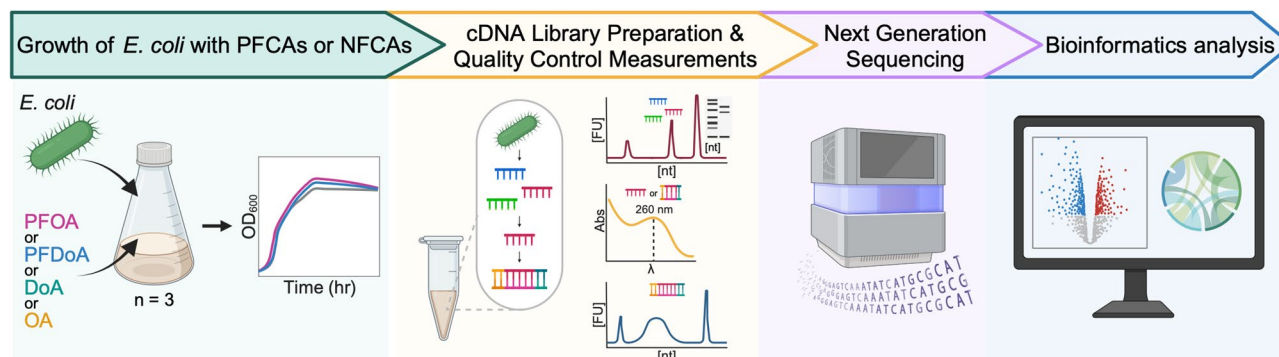


Fig. 1 Experimental and computational workflow. This study characterizes the PFCa-induced transcriptional response of *E. coli* during mid-exponential phase and stationary phase growth. The schematic diagram of experimental design and data processing provides an overview of the growth of *E. coli* with PFCAs or NFCAs, microbial growth measurements, and cDNA Library preparation and quality control measurements before next generation sequencing, bioinformatic data processing, and differential expression analysis. Additional culturing and sampling information can be found in SI Fig. 1.

phase, ferrous iron transport, amino acid metabolism, small regulatory RNAs during early stationary phase, and central metabolism, ribosome biosynthesis, molecular chaperones, sigma factors, and motility process of flagellar assembly and chemotaxis during late stationary phase. The transcription-level responses of *E. coli* to PFCAs presented in this study expand our knowledge of the molecular-level response to PFAS and could inform the development of future environmental monitoring and mitigation strategies.

Results and discussion

Culturing *E. coli* with 100 μmol/L of PFCa does not inhibit growth

To study the transcriptional responses of *E. coli* to PFAS, we first needed to understand the growth characteristics of *E. coli* in the presence of PFAS. From a sub-class of PFAS, two PFCAs, perfluorooctanoic acid (PFOA) and perfluorododecanoic acid (PFDoA), were selected as representative PFCAs commonly found in environmental contamination [12, 44] and to provide a comparison of chain length of PFCAs between 8 and 12 carbons, respectively (Fig. 2A). We aimed to select a concentration high enough to induce a measurable change in gene expression but low enough to avoid toxicity to the cells. We initially selected 10 μmol/L and 100 μmol/L of PFCAs to explore, as this concentration range has been used in transcriptomic studies of eukaryotic cells [38, 45] and fluoride concentrations within this range can stall cell division and growth of *E. coli* [46–48]. Although high, these concentrations are practically relevant as PFCAs, including PFOA, have been shown to accumulate up to 500 μmol/L in bacteria in the human gut [35]. *E. coli* was grown in M9 minimal medium supplemented with glucose and 10 μmol/L or 100 μmol/L of either PFOA or PFDoA for a period of 48 h at 37 °C (SI Fig. 1, Materials and Methods). The PFCAs were dissolved in dimethyl sulfoxide (DMSO), so to generate untreated control samples for

differential expression analysis, cells were cultivated in the same liquid medium with an equal concentration of DMSO not containing PFCAs. NFCAs, octanoic acid (OA) and dodecanoic acid (DoA) (Fig. 2A), were also included to compare the response of *E. coli* to fluorinated and non-fluorinated carboxylic acids. All sample groups were prepared in biological triplicate (SI Fig. 1). We monitored growth of *E. coli* in the presence and absence of PFCAs or NFCAs using optical density measurements at 600 nm (OD₆₀₀) at select time points (Fig. 2B; SI Fig. 2A, B, C) across 48 h. *E. coli* exhibited similar growth profiles for both 100 μmol/L (Fig. 2B; SI Fig. 2A) and 10 μmol/L (SI Fig. 2B, C) of PFOA, PFDoA, OA, and DoA, and a two-way mixed ANOVA confirmed no statistically significant difference in growth to the untreated control over time (Table SI 1). As both concentrations tested yielded similar growth profiles, we elected to collect samples for sequencing and downstream analysis from cells grown with 100 μmol/L of each compound.

Global transcriptional response of *E. coli* to PFCAs and NFCAs across the time course

Next, we collected samples for total RNA extraction and next generation sequencing (NGS) at 6 h, 24 h, and 48 h. Sampling times were selected to represent mid-exponential phase, the transition from exponential to stationary phase, and the end of stationary phase of bacterial growth. Gene expression naturally shifts between these growth phases [49]; therefore, we hypothesize PFCAs will further exaggerate the natural changes in expression. We extracted total RNA from three biologically distinct cultures of each sample type for commercial cDNA library preparation and sequencing (Materials and Methods). NGS generated a total of over 350 million reads with a mean quality score of 35.88 (Table SI 2).

We performed principal component analysis (PCA) of normalized data through DESeq2 methodology [50] to visualize variation in gene expression between the 45

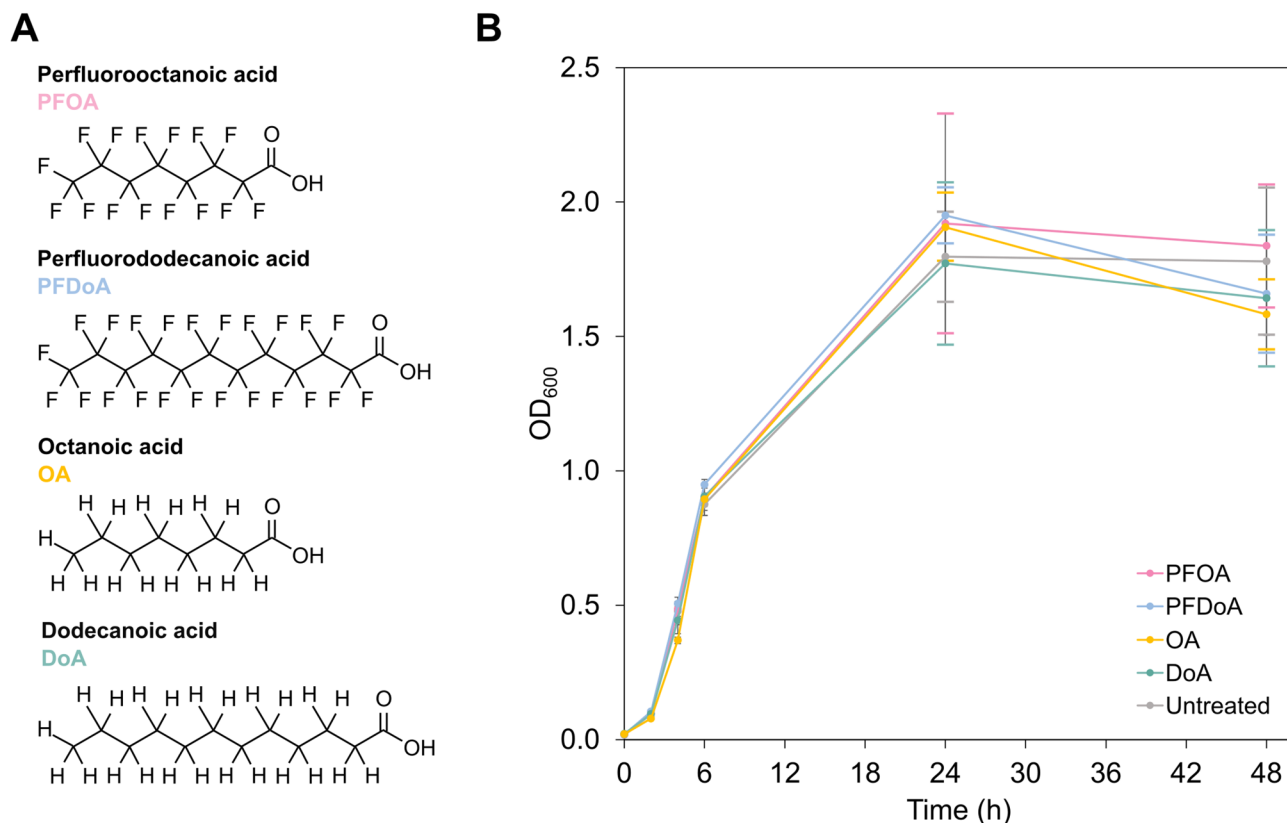


Fig. 2 Growth of *E. coli* in the presence of PFCA or NFCA. **A** Chemical structures of PFOA, PFDoA, OA, and DoA. **B** Growth of *E. coli* in M9 at 37 °C in the presence of 100 μmol/L of PFOA (pink), PFDoA, (blue), OA (yellow), or DoA (green) displayed as optical density measured at 600 nm (OD₆₀₀) over time (h). Untreated cells containing an equivalent final concentration of DMSO are displayed in gray. Error bars represent one standard deviation of the mean value of biological triplicates (Table SI 1) and are displayed in colors corresponding to PFCA or NFCA. Individual growth curves for each PFCA or NFCA are included in SI Fig. 2A.

samples in this study (SI Fig. 3). All transcriptomes first cluster with their respective growth phase as seen with PC1, implying an inherent temporal transcriptomic response. Transcriptomes of 24 h and 48 h samples had less variation and clustered closer to one another than to the 6 h transcriptomes, suggesting gene expression during the two points within stationary phase was more similar than mid-exponential phase at the time of sampling. These results demonstrate the global shift in gene expression is governed by a shift from active growth to cell survival and response to stress regardless of sample type. Additionally, PFOA samples clustered more closely to PFDoA samples than the untreated control samples throughout the time course (SI Fig. 3), indicating additional difference in gene expression was likely induced by PFCA. At 6 h and 24 h, NFCA transcriptomes clustered more closely to untreated control transcriptomes than PFCA transcriptomes, suggesting gene expression of NFCA and untreated samples were more similar compared to PFCA samples. PCA indicated a biological replicate of DoA at 48 h had a large variation in gene expression from the triplicate group (outlier); as a result,

DoA triplicate samples at 48 h were removed from further analysis.

We employed differential gene expression analysis to determine if PFCA induced a measurable change in *E. coli* gene expression over the time course. In this study, we consider genes to be differentially expressed if the adjusted p-value (padj) is less than 0.05. Additionally, we mark moderate and significant differential expression with absolute values of the log₂ fold change greater than or equal to 1.2 and 1.5, respectively. Untreated samples serve as the reference level for gene expression pairwise comparisons. The global transcriptional response of *E. coli* to PFOA and PFDoA demonstrates a measurable change in gene expression was induced by both PFCA throughout the time course (Fig. 3A, B). A similar number of genes were differentially expressed by PFOA and PFDoA at 6 h and 24 h (Fig. 4A). However, this trend diverges at 48 h, as PFOA induced the most differentially expressed genes and PFDoA induced the least. The considerable change in gene expression induced at 48 h by PFOA could be due to many factors, which we will explore in more detail in later sections. NFCA also induced a measurable change in gene expression when

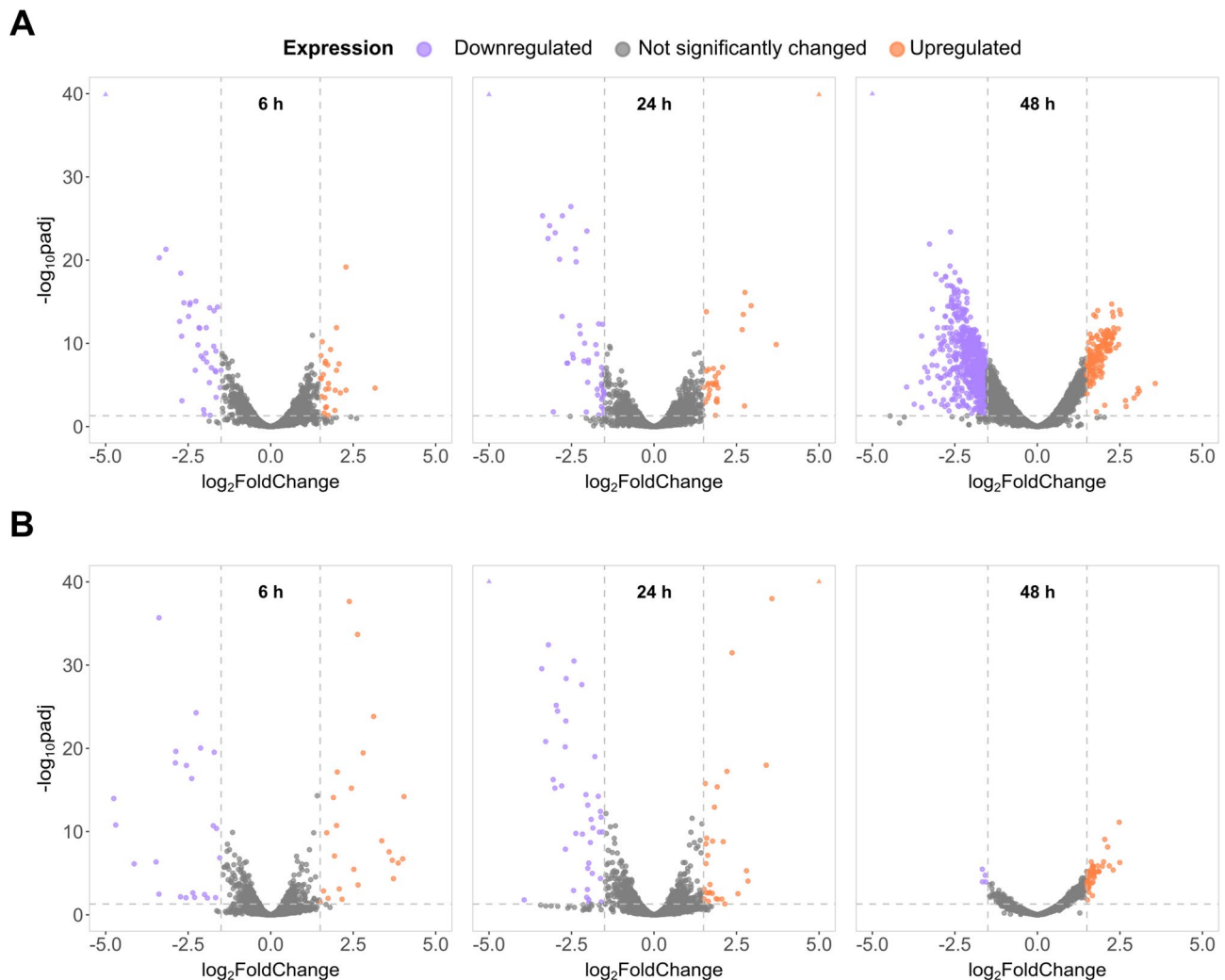


Fig. 3 Transcriptomic profiles of mid-exponential and stationary phase *E. coli* grown with PFCAs. Volcano plots show the global transcriptional response of *E. coli* to (A) PFOA and (B) PFDoA in comparison to an untreated control group at 6 h (left), 24 h (middle), and 48 h (right). Dashed lines represent a significance cutoff for differential expression of an adjusted p-value (padj) of less than 0.05 and absolute value of the \log_2 fold change greater than or equal to 1.5. Upregulated and downregulated genes are denoted by purple and orange, respectively, and genes not significantly changed by PFOA treatment are gray. Differentially expressed genes with \log_2 fold change and/or padj values outside of the plot limits are represented by orange or purple triangles in the upper corners of each plot, if applicable.

compared to the untreated control across the time course (Fig. 4B; SI Fig. 4A, B). *E. coli* grown with OA exhibited a similar pattern of expression to PFOA at 6 h and 24 h (SI Fig. 5A). However, PFOA induced differential expression of more than 700 genes at 48 h, in contrast, OA induced less than 40 genes (SI Fig. 5B), indicating differed response to fluorinated and non-fluorinated versions of the 8-chain compound. DoA had an opposite result from PFDoA, inducing differential expression in over 350 genes compared to over 50 genes at 6 h (Fig. 4A, B; SI Fig. 5C), further suggesting differed responses to fluorinated and non-fluorinated versions of the 12-chain compound.

We observed a temporal pattern to PFCA- and NFCA-induced differential expression, as the majority of genes were significantly changed at only one time point (Fig.

4C, D). Less than 30 and 15 genes were differentially expressed at multiple time points by PFOA and PFDoA, respectively (Table SI 3; Table SI 4). Only three genes, *gatD*, *glpA*, and *yeaR*, which are related to galactose metabolism and transport [51] and glycerol metabolism [52], were differentially expressed by PFOA at all time points in the study (Fig. 4C top; Table SI 3). Genes encoding formate hydrogenlyase subunits, iron transporters, and small regulatory RNAs were differentially expressed by PFOA at two of the three time points and will be discussed in later sections. Unlike PFOA, no genes were differentially expressed in *E. coli* by PFDoA at all time points (Fig. 4C bottom). Upon further investigation, nine genes, including the *trp* operon, downregulated by PFDoA at 6 h and 24 h, were also downregulated by PFOA and OA

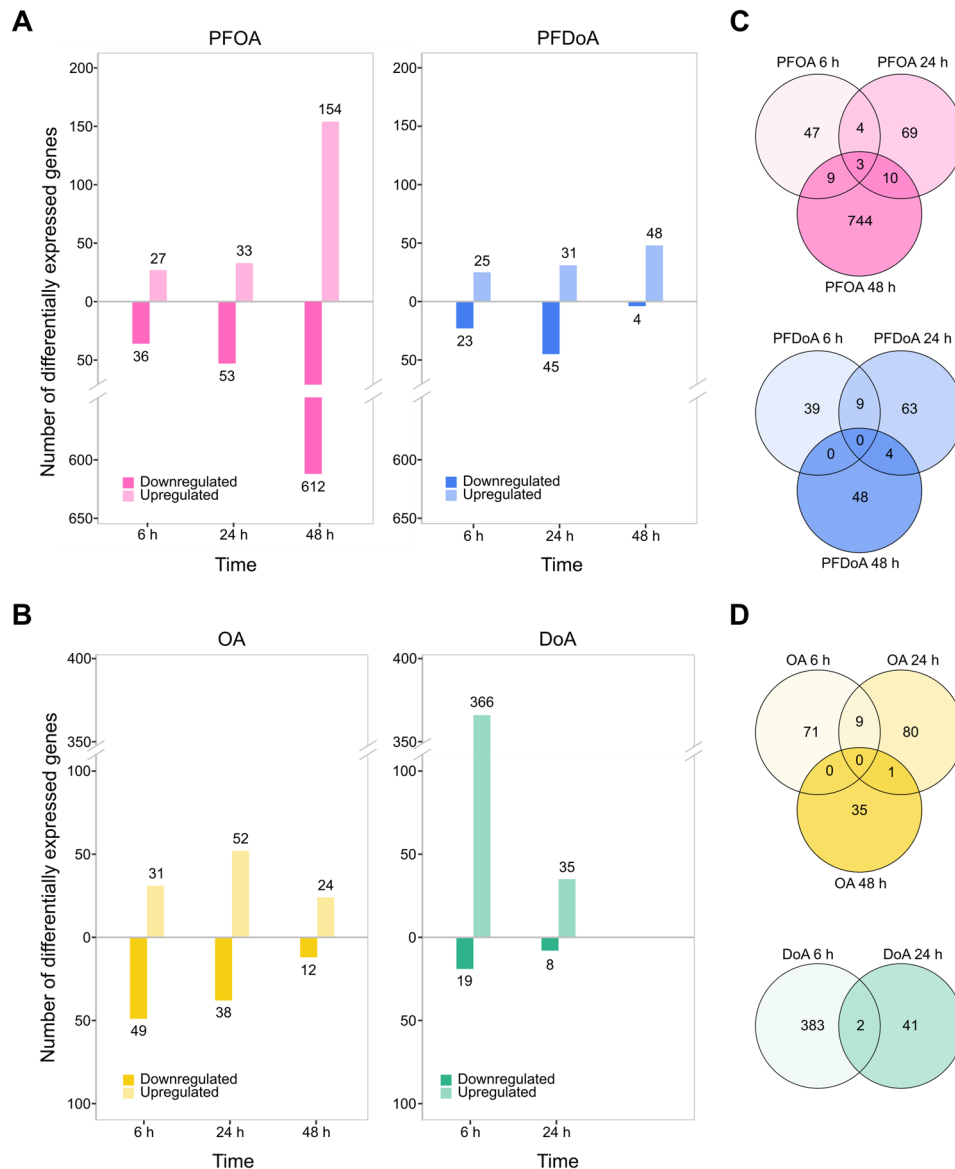


Fig. 4 Comparison of differential gene expression induced by PFCAs or NFCAs across the time course. The number of differentially expressed genes induced by **(A)** PFOA (pink, left), PFDoA (blue, right), **(B)** OA (yellow, left), and DoA (green, right) over the time course are shown by the height of each bar and label above or below the bar. Genes are considered differentially expressed if the absolute value of the log₂ fold change greater than or equal to 1.5 and the adjusted p-value less than 0.05. Upregulated genes are represented by the upper portion of the plot with lighter shaded bars as indicated by the legend. Downregulated genes are represented by the lower portion of the plot with darker shaded bars. Venn diagrams display the number of differentially expressed genes induced by **(C)** PFOA (top), PFDoA (bottom), **(D)** OA (top), and DoA (bottom) over the time course. Unions display genes differentially expressed by one PFCA or NFCA at more than one time point. Genes in the outer circles are only differentially expressed at a single time point by one PFCA or NFCA.

at 24 h and DoA at 6 h (SI Fig. 5D, E; Table SI 5), and will be discussed in a later section. Also discussed later, three of the four genes upregulated by PFDoA at 6 h and 24 h were also downregulated by PFOA at 24 h and 48 h and OA at 6 h (Table SI 5). These genes compose the ferrous iron transport operon, *feoABC*. Similar to PFOA, we observed a temporal pattern of OA-induced differential expression over the time course with minimal common expression between time points (Fig. 4B, D top; Table SI

6). Throughout the time course, PFOA and OA induced 13, 32, and 35 of the same genes at 6 h, 24 h, and 48 h, respectively (SI Fig. 5A, B; Table SI 7). These results suggest responses were triggered by the octanoic acid moiety regardless of fluorination. Additionally, DoA commonly induced differential expression in two genes, *prpC* and *ydeO*, involved in propionate catabolism [53] and regulation of the *gad* system [54], at 6 h and 24 h (Fig. 4D bottom; Table SI 8), similar to minimal shared expression

of 9 genes by PFDoA at 6 h and 24 h (Fig. 4C bottom; SI Fig. 5C; Table SI 4). Parallel to common expression between PFOA and OA, PFDoA and DoA induced differential expression in the same 19 genes at 6 h and 13 other genes at 24 h (SI Fig. 5C; Table SI 7). These results indicate differential expression induced by PFCAs or NFCAs is predominantly specific to a particular phase of growth. Lastly, we performed KEGG pathway and gene ontology (GO) enrichment analyses of differential expression datasets to assess whether key pathways were changed by PFCAs; however, there was minimal pathway-level enrichment across treatments and time points (SI File 1). We subsequently focus our analysis on select gene- and operon-level expression pathways with altered expression.

Transcriptional response of mid-exponential *E. coli* to PFCAs

Bacterial gene expression shifts significantly between exponential phase and stationary phase, reflecting the transition from active growth and energy production towards stress-mitigation and survival in resource-limited environments [49, 55]. We hypothesize PFCAs would alter gene expression differently during exponential phase and stationary phase. To better understand the response of *E. coli* to PFCAs at each growth phase within the study's time course, we sought to identify genes that were differentially expressed by PFOA and PFDoA (common responses) and the genes only changed by one PFCA (specific responses), starting at mid-exponential phase (6 h). Highlights of our results of the response of *E. coli* to PFCAs and NFCAs across the time course, discussed below, are illustrated in Fig. 5.

PFOA and PFDoA each induced differential expression of approximately 50 genes at 6 h (Fig. 4A; Table SI 3; Table SI 4). This is less than 2% of genes in the transcriptome, indicating growth in the presence of PFCAs does not seem to have a major impact on gene expression of mid-exponential *E. coli*. Only seven genes were differentially expressed by both PFCAs at 6 h (SI Fig. 5D). These genes, *nadA*, *msyB*, *hiuH*, *galS*, *adiY*, *yceK*, and *ymfQ*, encode a quinolinate synthase, acidic protein, hydroxyisourate hydrolase, DNA-binding transcriptional dual regulator and activator, and two uncharacterized proteins, respectively (Table SI 5). With roles in pyrimidine and purine metabolism, quinolinate synthase and hydroxyisourate hydrolase were also downregulated by PFOA and PFDoA at 24 h, indicating a sustained effect on gene expression. As a 4Fe-4 S cluster is required for activity of quinolinate synthase in NAD synthesis [56], downregulation of *nadA* could suggest a requirement for iron and sulfur that correlates with upregulation of sulfate assimilation and ferrous iron transport genes discussed in later sections. The DNA-binding

transcriptional dual regulator GalS was upregulated by PFOA at 6 h, but downregulated by PFDoA, suggesting *E. coli* exhibited a different response to the 8-chain PFCA compared to the 12-chain. Several of these genes were also downregulated in response to the NFCAs (Table SI 5; Table SI 7). For example, significant downregulation of *msyB* by both PFCAs and NFCAs implies some changes in gene expression were not specific to fluorinated compounds, but likely rather to carboxylic acids. The minimal common changes in gene expression at 6h implies *E. coli* utilized different mechanisms at mid-exponential phase to respond to PFOA and PFDoA.

During mid-exponential phase, *E. coli* differentially expressed several genes in response to PFOA but not PFDoA, including the formate regulon, a putative transporter YhjX, L-aspartate oxidase, L-alanine exporter, and small RNA RyjA (Table SI 3). Of particular interest, genes encoding components of the formate regulon, including the formate hydrogenlyase (FHL) complex, formate dehydrogenase H, and the hydrogenase pleiotropic *hyp* operon [57], were significantly downregulated (Figs. 5A and 6A; Table SI 9). The FHL complex is essential to fermentative H₂ production in *E. coli* during mixed-acid fermentation. At low extracellular pH and high levels of re-imported formate during stationary phase, the FHL complex is activated to disproportionate accumulated formate to hydrogen and carbon dioxide [58, 59]. We found the formate channel, encoded by *focA*, that transports formate from the cytoplasm during exponential phase under physiological pH, was not differentially expressed at 6 h by either PFCA or NFCA, indicating these compounds did not induce more or less formate transport than the untreated control. However, formate dehydrogenase H, encoded by *fdhF*, and the *hyc* operon, composed of genes encoding the cytoplasmic domain subunits, *hycBEFG*, and membrane domains, *hycCD*, of the FHL complex, plus the transcriptional regulator, *hycA*, chaperone, *hycH*, and protease, *hycI*, were downregulated by PFOA at 6 h (Fig. 6A; Table SI 9). Additionally, *hycBCDE* were also significantly downregulated by PFOA at 48 h, indicating the change in expression of these four genes was not unique to mid-exponential phase. Four genes of the *hyp* operon, *hypABCD*, encoding products involved in nickle:iron hydrogenase maturation [57, 60], and a gene encoding a putative transporter predicted to function as an oxalate:formate antiporter, *yhjX* [61, 62], were also downregulated at 6 h by PFOA but not differentially expressed by PFDoA or either NFCA. Downregulation of formate regulon genes, unfavorable reaction conditions in an aerobic environment, and the unlikely occurrence of common inducing factors like acidic pH, the absence of nitrates, and unlikely PFOA-induced formate accumulation during mid-exponential phase, suggests forward conversion of formate was possibly prevented [58]. These

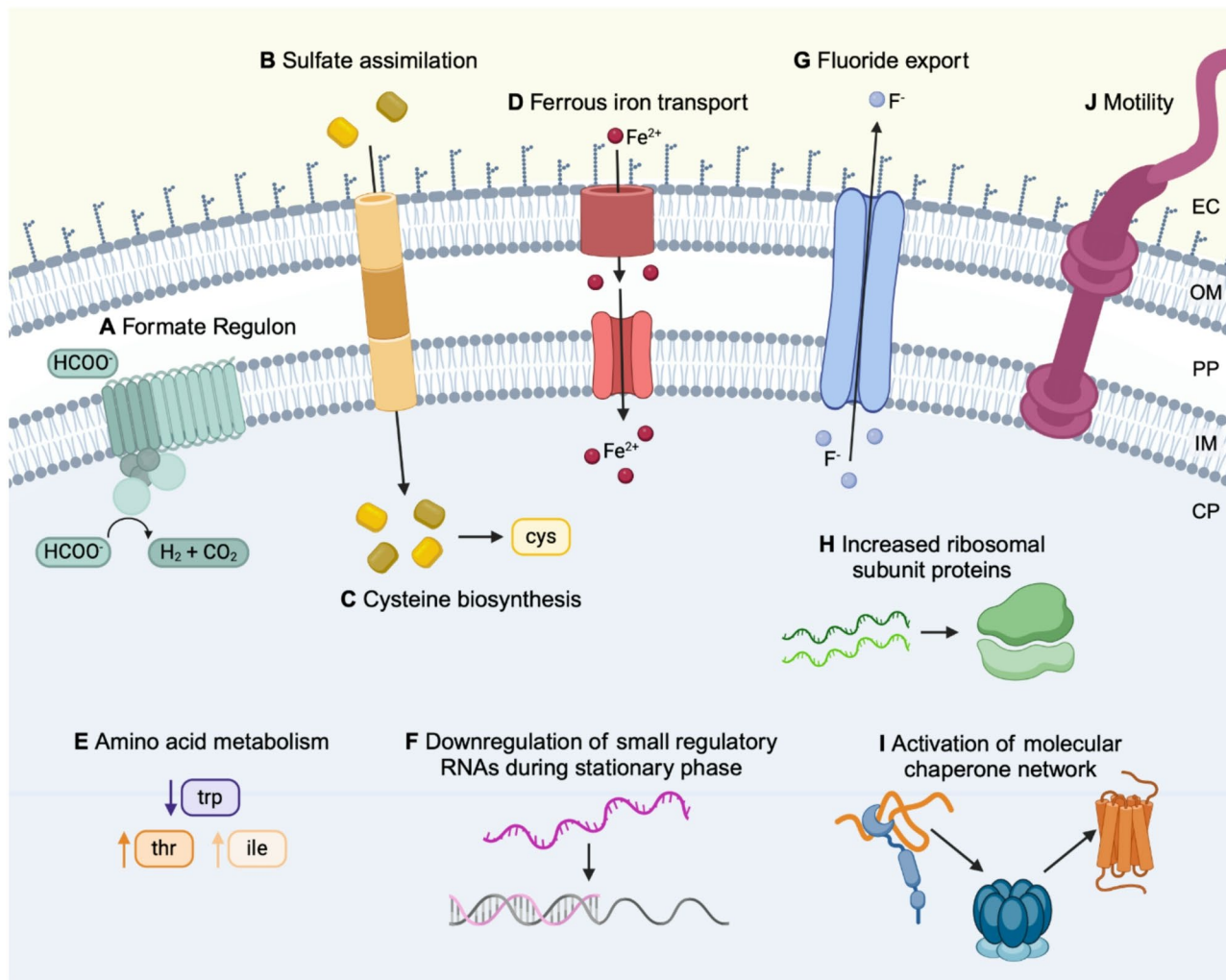


Fig. 5 Schematic of key biological processes with altered gene expression by PFCAs across the time course. These processes containing differentially expressed genes are highlighted in the results and discussion. The formate regulon (A), sulfate assimilation (B), and cysteine biosynthesis (C) are discussed in the mid-exponential phase section (Fig. 6). Ferrous iron transport (D), amino acid metabolism (E), and small regulatory RNAs (F) are discussed in the early stationary phase section (Fig. 7). Fluoride export (G), ribosomal subunit proteins (H), the molecular chaperone network (I), and motility processes (J) are discussed in the late stationary phase section (Fig. 8). The cytoplasm (CP), Inner membrane (IM), periplasm (PP), outer membrane (OM), and extracellular environment (EC) are labeled on the right side of the schematic. The CP, PP, and EC have blue, white, and yellow backgrounds, respectively.

results further signify a specific response to PFOA that differs from routine transport and conversion of formate under physiological conditions. Lastly, formate is a degradation product of PFOA, and additional measurements would be needed to determine if formate ions from PFOA were present in the cultures.

During mid-exponential phase, PFDoA induced overexpression of genes involved in sulfate and thiosulfate assimilation and L-cysteine biosynthesis (Figs. 5B and C and 6B; Table SI 4; Table SI 10). Sulfate assimilation is crucial for the growth and survival of *E. coli*, as sulfur is needed to synthesize cysteine and many cofactors and is important for cellular redox balance [63]. Sulfate and thiosulfate transporters are often overexpressed in *E. coli* when intracellular sulfur is limited, and uptake

of extracellular sulfate is needed [64]. Newly assimilated sulfur-containing intermediates are then converted to cysteine [65]. The sulfate/thiosulfate ATP-binding cassette (ABC) transporter complex, *cysPUWA*, was significantly upregulated with \log_2 fold changes greater than 2.75 by PFDoA at 6 hr (Fig. 6B; Table SI 10). This was not observed with PFOA or DoA. Genes encoding the transporter's periplasmic protein, *cysP*, and inner membrane subunit, *cysU*, were also significantly upregulated by OA at 6 hr, indicating possible uptake of sulfate was induced by OA as well (SI Fig. 5D). In a second path for sulfur assimilation, genes, *tsuAB*, in a recently characterized thiosulfate ion uptake mechanism [66], were also upregulated by PFDoA at 6 hr (Fig. 6B), but were not significantly changed by DoA. These results suggest

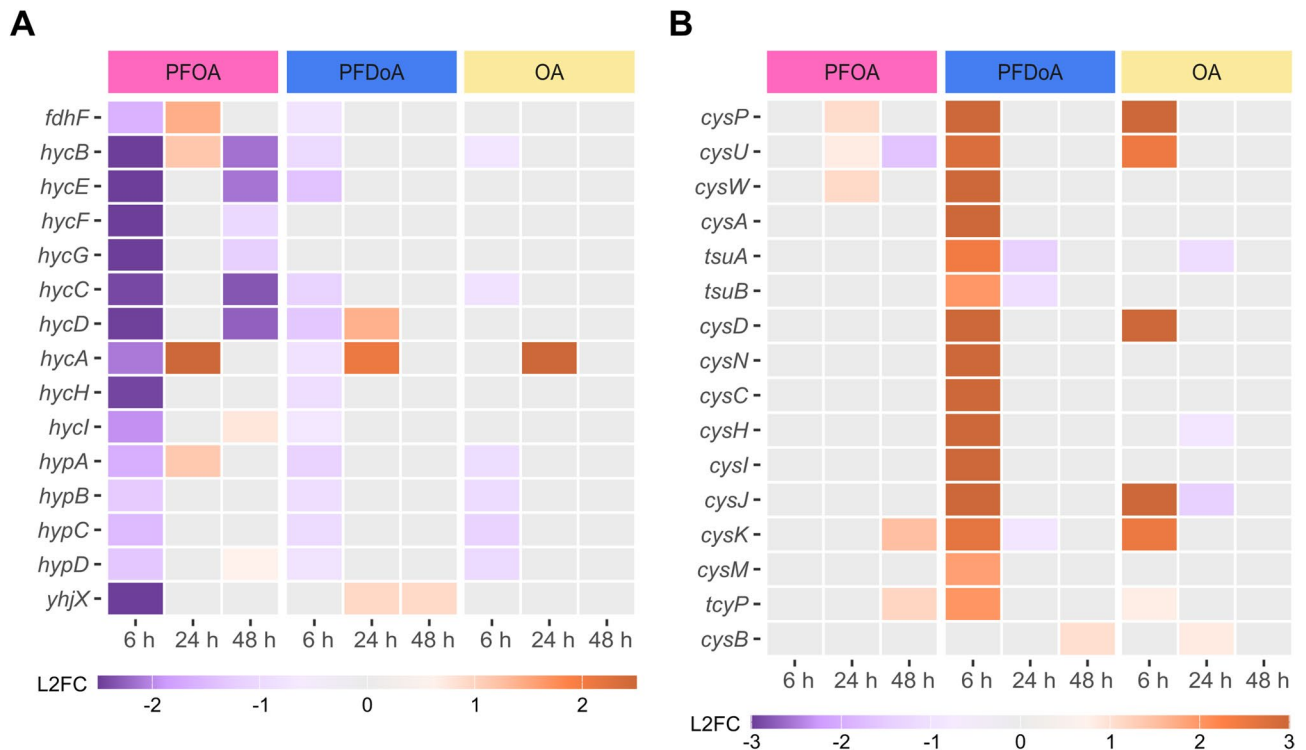


Fig. 6 Select genes with differential expression at 6 h and their temporal change. Heatmaps display differential expression of select genes ($\text{padj} < 0.05$) involved in **(A)** the formate regulon and **(B)** sulfate assimilation and cysteine biosynthesis. Expression is represented by \log_2 fold change (L2FC) within a gene compared to untreated control in a purple to orange scale displayed by legend color bar below each heatmap. Note heatmap color bars are different scales in **(A)** and **(B)** to best highlight differences. PFOA or NFCA treatment is represented by color coded bars at the top of the heatmaps: PFOA (pink), PFDoA (blue), and OA (yellow). Genes with no statistically significant change in expression are represented by gray boxes. DoA did not induce significant differential expression ($\text{padj} < 0.05$, $|\text{L2FC}| > 1.2$) of the displayed genes across time points (Table SI 9, 10).

PFDoA induced a specific response to utilize this mechanism for thiosulfate ion uptake, and the response was likely triggered by the 12-chain PFCA. Following sulfate and thiosulfate uptake, the genes encoding enzymes that catalyze the activation and subsequent reduction of sulfate to intermediates, sulfite and sulfide, were upregulated by PFDoA. The sulfate activation operon, *cysDNC*, responsible for chemical activation of sulfate to adenosine 5'-phosphosulfate (APS) by ATP sulfurylase and APS kinase and the gene cluster, *cysHIJ*, encoding APS reductase and sulfite reductase subunits, responsible for the reduction of APS to sulfite and sulfite to sulfide [67, 68], respectively, were overexpressed by PFDoA (Fig. 6B).

In addition to upregulation of sulfur-containing compound transporters and redox enzymes, unsurprisingly, cysteine synthases, *cysKM* [65], and an inner membrane L-cystine (dimeric cysteine) transporter, *tcyP*, were significantly upregulated by PFDoA at 6 h (Figs. 5B and 6B). Furthermore, when grown on minimal medium, as done in this study, TcyP functions as the main importer of L-cystine [69] and is activated when intracellular cysteine is low [65]. These changes in gene expression could indicate an increase requirement for cysteine through sulfate assimilation or direct import in response to PFDoA.

Lastly, the gene encoding the regulatory protein CysB, which drives the sulfur limitation response in *E. coli*, was not differentially expressed by any PFCA or NFCA treatment in this study [67, 70]. It is possible the gene was overexpressed at an early point in exponential phase as the genes it regulates were overexpressed by PFDoA at the mid-exponential mark or has consistent expression. Overexpression of sulfate and thiosulfate assimilation components and cysteine biosynthesis enzymes by PFDoA, indicates PFDoA could be negatively impacting redox balancing and in turn, stimulating an increased requirement for sulfur-containing compounds like cysteine during mid-exponential phase.

Transcriptional response of early stationary phase *E. coli* to PFCAs

During stationary phase, bacteria modulate gene expression by simultaneously activating essential genes for survival and stress mitigation, while preventing transcription of unnecessary genes in a nutrient-deficient environment. Additional stress induced by the prolonged presence of PFCAs may further modify gene expression during stationary phase when compared to mid-exponential phase. Unlike mid-exponential phase, the number of genes

differentially expressed specifically by PFOA or PFDoA during stationary phase at 24 h was minimal (SI Fig. 5D, E). PFOA induced specific changes in gene expression of genes encoding cytochrome bo3 subunits, biotin biosynthesis enzymes, and transporters for iron and tryptophan (Table SI 3), whereas PFDoA induced changes in gene expression of inner membrane proteins and the small regulatory RNA GadY (Table SI 4). In contrast to minimal common responses observed at 6 h, PFOA and PFDoA induced differential expression of the same 49 genes at 24 h (SI Fig. 5D, E, F; Table SI 5). Products of these genes have roles in ferrous iron transport (Fig. 7A), amino acid metabolism (Fig. 7B), and small RNA regulation (Fig. 7C). Common changes in gene expression suggest these responses are not specific to a particular length of PFCAs, but to the PFCAs explored within the scope of this study. Expression of 24 of the 49 genes were also significantly changed by OA at 24 h and only 10 were changed by DoA (SI Fig. 5E; Table SI 5; Table SI 7), indicating those genes likely have a larger role regarding carboxylic acids in general, rather than fluorination.

As iron is an essential nutrient and cofactor in various enzymes, several iron acquisition systems and regulators have evolved to maintain intracellular iron homeostasis [71, 72]. Our analysis revealed genes encoding components of iron uptake transport mechanisms were differentially expressed in response to PFCAs (Fig. 5D; Table

SI 5; Table SI 11). One operon *feoABC*, which encodes ferrous iron (Fe^{2+}) transporters [73], was significantly upregulated at 24 h and 48 h by both PFOA and PFDoA (Fig. 7A; SI Fig. 5F). The operon was also upregulated at 24 h by OA (Table SI 11), implying the elevated response could be stimulated by the carboxylic acid moiety. Upregulation of *feo*, in combination with no significant change in the expression of upstream Fur and Fnr transcripts, the ferric iron (Fe^{3+}) transcriptional regulator and activator [74, 75], suggests PFCAs induce a requirement for intracellular ferrous iron during stationary phase. We hypothesize this is due to preference for the soluble ferrous form in comparison to insoluble ferric form at the pH of the culture. Moreover, the level of free iron could increase via *feo* transport because a putative Fur-regulated inhibitor, *rhyB* [76, 77], was downregulated by PFOA at 48 h. Additionally, fluoride exposure can deplete active forms of metal ions, including iron, through formation of stable metal-fluoride complexes, therefore, triggering cells to increase free metal ion concentration [78, 79] to maintain homeostasis. Siderophores, secreted ferric iron scavengers [80, 81], were not employed because the enterobactin gene cluster and associated transporters were moderately downregulated at 48 h by PFOA (Table SI 11). However, genes, *exbB* and *exbD*, in the associated TonB energy-transducing complex [82] were upregulated by PFOA and PFDoA at 48 h (Fig. 7A). The *efeUOB*

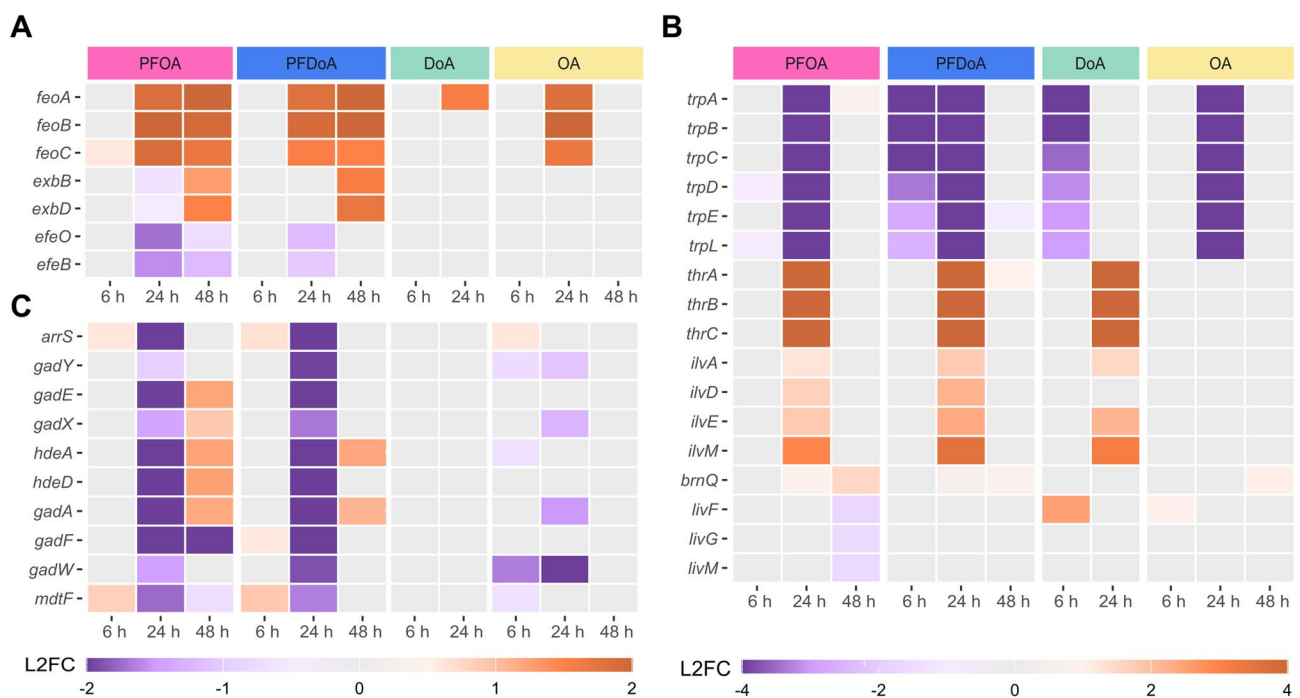


Fig. 7 Select genes with differential expression at 24 h. Heatmaps display differential expression of select genes ($p_{adj} < 0.05$) involved in (A) ferrous iron transport, (B) amino acid metabolism, and (C) small regulatory RNAs across the time course. Expression is represented by \log_2 fold change (L2FC) within a gene compared to untreated control in a purple to orange scale displayed by legend color bar below each heatmap. Note panels A and C share the same L2FC scale, which differs from panel B. PFOA or NFCA treatment is represented by color coded bars at the top of the heatmaps: PFOA (pink), PFDoA (blue), DoA (green), and OA (yellow). Genes with no significant change in expression are represented by gray boxes (Table SI 11).

operon encoding a ferrous iron transporter complex is not fully functional in *E. coli* MG1655 due to a frameshift mutation in *efeU* [83], but the genes encoding periplasmic proteins, *efeO* and *efeB*, were also downregulated by both PFCAs at 24 h. Additionally, PFOA-induced downregulation of genes encoding various cytochromes (Table SI 11) during stationary phase could suggest limited available iron for incorporation into heme groups [84–86]. These results further signify a specific preference and need for ferrous iron uptake by the *feo* operon during stationary phase and likely limited availability for incorporation in key components like cytochromes [85].

During stationary phase, gene expression is altered to meet metabolic requirements including the adjustment of amino acid metabolism [87, 88]. Genes encoding the *trp* operon, the *thr* operon, isoleucine synthesis components (*ilvADE* and *ilvM*), and transporters of branched-chain amino acids (*brnQ* and *livFGM*) were differentially expressed by PFOA and PFDoA during stationary phase (Figs. 5E and 7B; Table SI 11). Notably, differences in gene expression between PFCa samples and the untreated controls of the *trp* and *thr* operons were some of the largest in this study, with \log_2 fold changes less than -5.3 and greater than 4.6 , respectively. Downregulation of the *trp* operon would suggest an effort to route metabolic flux towards optimal parts of central metabolism or amino acid biosynthesis pathways (SI Fig. 6) [89], in order to adapt to high levels of intracellular tryptophan or related PFCa-induced stress. Alternatively, upstream precursors to the *trp* operon, like chorismate [90], may not have been available, and as a result, the operon was underexpressed. The *trp* operon was also downregulated by DoA at 6 h and OA at 24 h (Fig. 7B; Table SI 11), indicating the change in gene expression was possibly prompted by the octanoic acid moiety regardless of the presence or absence of fluorination. Moreover, downregulation of tryptophan symporters, *mtr* and *tnaB*, at 24 h and no change in expression of the general aromatic acid transporter, *aroP*, imply extracellular tryptophan was likely not imported into cell (Table SI 11). Upregulation of threonine and isoleucine biosynthesis genes could be a direct result of carbon flux redirection from upper metabolism, and the synthesized amino acids [91, 92] could be used in processes to mitigate stress and sustain growth during nutrient-limited stationary phase.

Small regulatory RNAs (sRNAs) help modulate gene expression during stationary phase and under environmental stress by stabilizing specific mRNAs and stimulating translation [93]. At 24 h, 10 sRNAs, their corresponding mRNAs targets, and flanking genes were downregulated by PFOA and PFDoA (Figs. 5F and 7C; Table SI 11). A handful of these genes remained downregulated by PFOA at 48 h. In this study, this response was fairly specific to PFCAs, as only four of these genes

were differentially expressed by NFCAs. Also, the genes encoding RNA-binding proteins Hfq and ProQ were minimally overexpressed by PFOA at 48 h with \log_2 fold changes of approximately one. These proteins work in tandem with sRNAs to bind target mRNAs and provide intracellular stability [94]. Downregulation of antisense sRNAs genes, *arrS* and *gadY*, the corresponding mRNAs that they target, *gadE* and *gadX*, and flanking genes, *hdeAD*, *gadAFW*, and *mdtF*, during stationary phase by PFOA and PFDoA (Fig. 7C), suggests possible energy conservation and resource reallocation to critical survival pathways [93, 95] in response to PFCAs. Lastly, *arrS* and *gadY* products have essential roles in acid resistance regulation [95], and downregulation of these sRNAs at 24 h suggests PFCAs either do not significantly induce acid stress compared to the untreated control, or the activation of pH homeostasis mechanisms is too costly due to nutrient limitation during stationary phase.

Transcriptional response of late stationary phase *E. coli* to PFCAs

To compare the transcriptional response of *E. coli* to PFCAs at different points within stationary phase, we wanted to understand how differential expression patterns induced at 48 h differed from patterns at 24 h. At 48 h, PFOA and PFDoA upregulated 28 common genes that encode the 50 S ribosomal subunits, the DNA-binding transcriptional repressor LsrR, and Ton complex subunit ExbD (Table SI 5; SI Fig. 5E, F). Seventeen of these genes were also moderately upregulated by OA (Table SI 7), with a \log_2 fold change of at least 1.4, indicating differential expression may not be specific to PFCAs. We observed specific changes in gene expression of cold shock proteins and putative phosphotransferase system enzymes by PFDoA at 48 h (Table SI 4).

In contrast to the minor response to PFDoA, PFOA induced the largest and broadest change in gene expression in the entire study at 48 h. For this timepoint, we observed a change in gene expression of a fluoride exporter, central metabolism enzymes, ribosomal proteins, molecular chaperones, autoinducer-2, and motility components induced by PFOA (Fig. 8; SI Fig. 6; Table SI 3; Table SI 12; Table SI 13, Table SI 14).

High concentrations of environmental fluoride can inhibit metabolism, ribosomes, and protein processing, in addition to altering pH and inducing oxidative stress in *E. coli* [46, 79]. Similar molecular mechanisms of oxidative stress along with membrane permeability have been demonstrated by PFAS toxicity [39, 96, 97]. Exporters, including the selective Fluc family fluoride ion channels, mediate fluoride resistance and protect bacteria against toxicity [98]. The *crcB* gene of *E. coli* encodes a Fluc fluoride transport channel to expel fluoride out of the cell [46]. Moderate upregulation, \log_2 fold

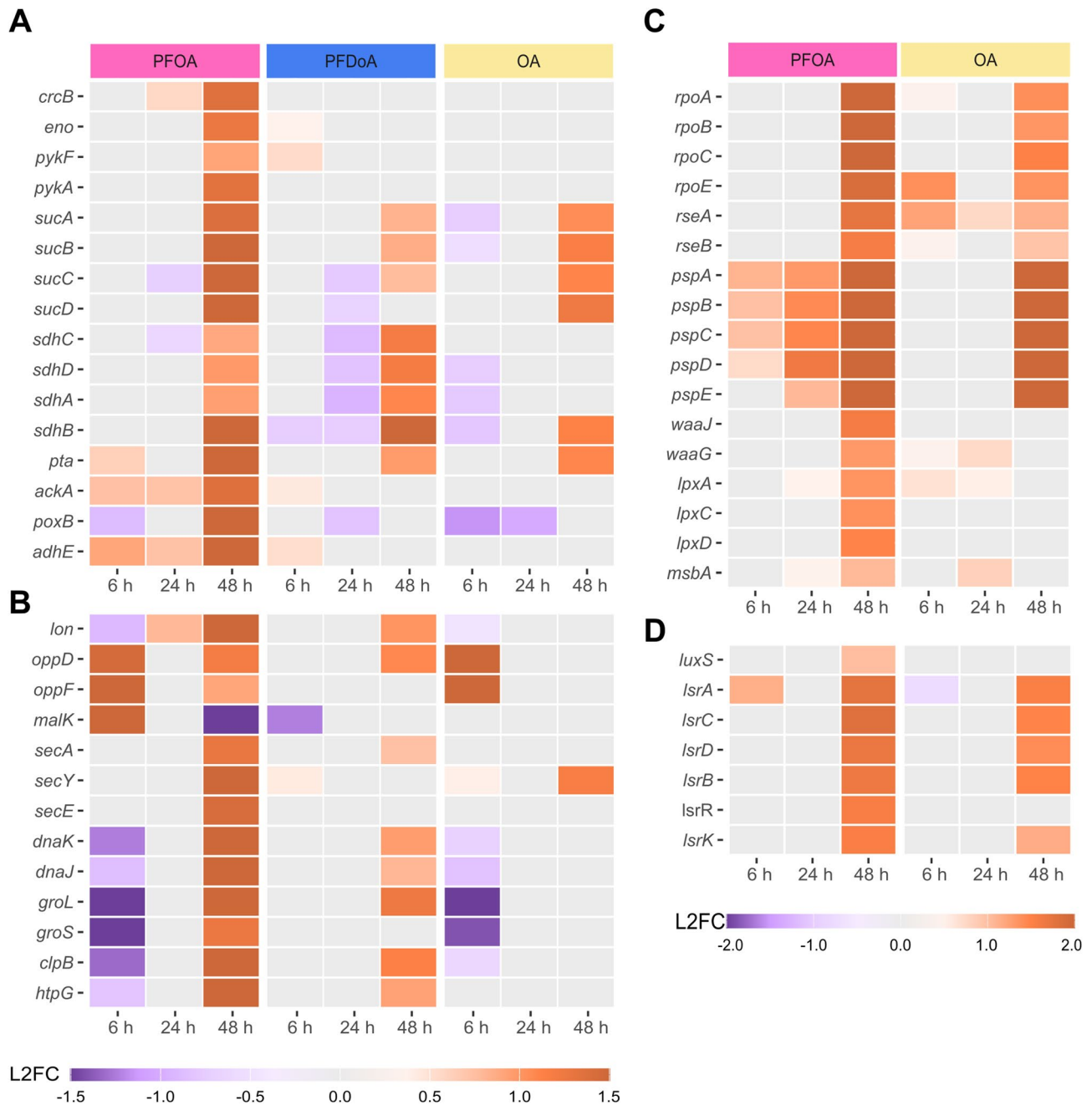


Fig. 8 Select genes with differential expression at 48 h. Heatmaps display differential expression of select genes ($p_{adj} < 0.05$) encoding (A) a fluoride exporter and metabolic enzymes, (B) ATPases and the molecular chaperone network, (C) sigma factors and envelope stress response, and (D) the AI-2 signaling system at select time points in the time course (6, 24, 48 h). Expression is represented by \log_2 fold change (L2FC) within a gene compared to untreated control in a purple to orange scale displayed by legend color bar below each heatmap. Note heatmaps in (A) and (B) share the same L2FC scale and heatmaps in (C) and (D) share a separate scale. PFOA or NFOA treatment is represented by color coded bars at the top of the heatmap: PFOA (pink), PFDoA (blue), and OA (yellow). Genes with no significant change in expression are represented by gray boxes. PFDoA and DoA did not induce significant differential expression ($p_{adj} < 0.05$, $|L2FC| > 1.2$) of the displayed genes across time points in C, D and A-D, respectively (Table SI 12-14).

change of 1.4, of *crcB* at 48 h by PFOA suggests a need to export intracellular fluoride potentially accumulated from PFOA throughout the time course (Figs. 5G and 8A; Table SI 12). Previous studies have observed the partitioning of PFAS with varying chain length into bacterial

membranes and subsequent increase in membrane fluidity [96, 97]. In addition, *E. coli* has mechanisms to indiscriminately uptake fluoride through membrane ion channels or porins [46, 99]. These results suggest a potential chain-length difference in PFCA uptake and

subsequent fluoride accumulation, as *crcB* was not differentially expressed by PFD_oA at 48 h. Additional measurements will be needed to further explore this result.

Key components in various biological processes including glycolysis and the citric acid cycle (TCA) enzymes, ribosomal proteins, ATPases, and molecular chaperones were also upregulated at 48 h by PFOA (Fig. 8A; Table SI 12). Vital for bacterial growth, genes encoding glycolytic enzymes enolase, *eno*, and pyruvate kinases, *pykF* and *pykA*, were moderately upregulated by PFOA at 48 h (Fig. 8A; SI Fig. 6), while *ppsA*, the phosphoenolpyruvate (PEP) synthetase encoding gene, which catalyzes a reverse reaction from pyruvate to PEP, was not differentially expressed. Enolase and kinases can be inhibited by micromolar amounts of fluoride as the ion can complex to metal ion active sites displacing the electronegative substrate [98, 100]. Fluoride inhibition of the activity of these key enzymes in central metabolism can result in the suspension of bacterial growth until fluoride is removed [46, 101]. Upregulation of glycolytic enzymes at 48 h provides further evidence of a specific response to possible fluoride accumulation from PFOA and export with *crcB*. Moreover, additional measurements within and beyond the time course could show if *crcB* mediated export of fluoride alleviates possible inhibition. The *sucABCD* operon, encoding TCA enzymes, was significantly upregulated by PFOA at 48 h, whereas the upstream *sdhCDAB* operon, encoding succinate dehydrogenase, was moderately upregulated, log₂ fold change of approximately 1.0 and 1.2, by PFOA at PFD_oA, respectively (Fig. 8A; SI Fig. 6). Conversion of succinyl-CoA to succinate generates GTP indirectly contributing to energy production [102]. Succinyl-CoA also plays a role in peptidoglycan biosynthesis by generating precursor lysine and diaminopimelate [103]. Overexpression key metabolic enzymes and the fluoride exporter at 48 h, suggests *E. coli* could be recovering from possible fluoride inhibition during stationary phase. In connection to partial upregulation of glycolytic and TCA enzymes, genes encoding products of mixed-acid fermentation were also overexpressed in response to PFOA at 48 h (Fig. 8A; SI Fig. 6). Upregulation of genes (*pta*, *ackA*, *poxB*, *adhE*) encoding enzymes for pyruvate and acetyl-CoA conversion to acetate, succinate, and ethanol, in addition to activation of upstream enolase further corroborates a possible restart of central metabolism [104]. Furthermore, production of mixed-acid fermentation products and TCA intermediates, implies an essential metabolic requirement for survival in nutrient-limited stationary phase exacerbated by PFOA.

Growth in the presence of PFCAs induced the overexpression of ribosomal proteins at 48 h (Fig. 5H). Forty-two genes encoding 50 S and 30 S ribosomal protein subunits [105] were upregulated by PFOA at 48 h, and 17 of which were also upregulated by PFD_oA (Table SI 12).

Though ribosome biogenesis can be reduced in response to nutrient limitations and stress [106], and fluoride can inhibit protein synthesis [78], the observed increase in gene expression of ribosomal proteins could suggest a requirement for machinery to translate new proteins in response to PFCAs late in stationary phase. These results also suggest an increase in ribosome biogenesis in response to the possible decrease in fluoride concentration by *crcB*-mediated export of fluoride. This observation is corroborated by similar findings in a proteomics study of upregulation of ribosomal proteins in anaerobic *E. coli* supplemented with PFOA [39].

Several ATPases, including transporters and molecular chaperones, were also upregulated by PFOA at 48 h despite no significant change in expression at 24 h (Fig. 8B; Table SI 12). ATPases are integral to survival and stress adaptation, and PFOA-induced stress or inhibition by fluoride [79, 107, 108] could lead to disruption of energy metabolism and cellular homeostasis. Upregulation of the ATP-dependent Lon protease (Fig. 8B), with roles in metabolic regulation, protein quality control, and degradation of abundant ribosomal proteins [109, 110], at 48 h, implies a possible need for the protease to degrade misfolded or abnormal proteins to supply amino acids for protein synthesis during stationary phase [111]. Gene expression of ABC transporter ATPases in the oligopeptide transport system, *oppD* and *oppF*, and maltose transport, *malK* [112], varied throughout the time course. Initially, the ATPases were upregulated at 6 h, not differentially expressed at 24 h, and moderately upregulated again at 48 h by PFOA (Fig. 8B). Likewise, a proteomics study found upregulation of the same oligopeptide-binding proteins in *E. coli* cultivated with PFOA [39]. The gene encoding the ATPase SecA and other essential components of the bacterial Sec translocase, *secYG* [113, 114], were also upregulated at 48 h (Fig. 8B; Table SI 12). As protein secretion is essential in bacteria, the Sec system provides a form of transmembrane translocation to ferry polypeptides from the cytoplasm across the cytoplasmic membrane into the periplasm [115, 116]. Overexpression of these genes suggests possible PFOA-induced intracellular protein accumulation and likely saturation of existing Sec-translocases at 48h. Moreover, if fluoride possibly inhibited SecA, upregulation at 48 h implies an increased abundance of SecA transcripts, similar to other ATPases discussed. Although the gene encoding SecB, the protein secretion chaperone that interacts with the Sec translocase, was not even moderately upregulated with a log₂ fold change of 0.81, other molecular chaperones may assist in protein processing in response to PFOA.

Bacteria employ molecular chaperones as regulators and facilitators of protein folding, transport, and control to maintain cellular homeostasis, especially during environmental stress. ATP-dependent molecular chaperones

DnaK, GroEL, and trigger factor (TF) along with cochaperones DnaJ, GrpE, and GroES coordinate the folding of newly synthesized cytosolic proteins in *E. coli* [117]. Genes encoding the chaperone network, *dnaKJ*, *groLS*, *clpB*, and *hspG*, were highly overexpressed by PFOA at 48 h (Figs. 5I and 8B; Table SI 12). Conversely, the genes were initially downregulated by PFOA at 6 h. Molecular chaperones are overexpressed in response to other environmental stressors such as temperature, heavy metals, limited nutrients, and chemical pollutants [118, 119]. Upregulation of molecular chaperones genes during stationary phase suggests stress-induced activation in reaction to the presence of PFOA. This is consistent with existing literature that has found PFAS can destabilize and denature proteins [120, 121]. Although PFD_oA induced moderate overexpression of select chaperones at 48 h (Fig. 8B), significant upregulation by PFOA of the chaperone network indicates a chain-length dependent response. Moreover, these results also suggest a specific response to PFCAs as there was no significant change in gene expression induced by either NFCA at 48 h.

Further analysis revealed PFOA triggered various stress responses as genes encoding sigma factors, components of envelope stress response mechanisms, and motility systems of flagellar assembly and chemotaxis were differentially expressed (Fig. 8C, D; SI Fig. 7). RNA polymerase (RNAP) core enzyme subunits, *rpoA* and *rpoBC*, RNAP sigma factors, *rpoE*, *rpoH*, *rpoF/fliA*, and *rpoS*, and RpoE regulators, *rseABC*, were highly upregulated by PFOA and only moderately upregulated by OA at 48 h (Fig. 8C; Table SI 13). As these genes have regulatory roles in the transcription of genes involved in outer membrane stress response, heat shock, flagellar assembly, and stationary phase gene expression, respectively, overexpression suggests heightened regulation of mechanisms employed to mitigate possible stress of PFCAs and NFCAs [122–124]. Similar to RNAP and sigma factors, the phage-shock-protein (Psp) operon, *pspABCD*, was also upregulated by PFOA and OA at 48 h (Fig. 8C; Table SI 13). In contrast to OA, the magnitude of overexpression of the operon by PFOA increased over the time course. As the Psp system can be initiated by a damaged inner membrane [125] and Sec translocase overload [126], an increase in expression throughout the time course by PFOA suggests use of the regulation mechanism to combat possible envelope stress. Our results show additional evidence of PFOA-induced envelope stress as the lipopolysaccharide (LPS) gene clusters responsible for the synthesis of the core oligosaccharide structure, *rfa*, and the lipid A soluble proteins, *lpxA*, *lpxC*, and *lpxD*, and the ATP-binding LPS transporter, *msbA* [127], were moderately upregulated at 48 h (Fig. 8C; Table SI 13). Overexpression of these genes may suggest the need to synthesize LPS components to maintain the outer membrane, despite the high energetic

cost. Previous studies have shown that PFAS partition into lipid bilayers and disrupt bacterial membranes, leading to increased permeability [96, 97, 128]. Our results suggest *E. coli* is employing several mechanisms to mitigate envelope stress, likely from PFOA.

To adapt to limited resources in stationary phase and respond to external stressors, bacteria will downregulate high energetic-cost processes like motility to reallocate resources to survival [129, 130]. We observed downregulation of genes encoding components involved in flagellar assembly, chemotaxis, and extracellular polysaccharide (EPS) biosynthesis at 48 h by PFOA (Figs. 5J and 8D; SI Fig. 7; Table SI 14). These results suggest PFOA could be inducing a transition from a sessile state towards possible biofilm formation, therefore reducing motility via downregulation of flagellar assembly, as an indirect effect, in order to conserve energetic resources. Notably, DoA-induced upregulation of the same flagellar assembly and chemotaxis genes during mid-exponential phase (SI Fig. 7; Table SI 14) suggests these processes may have been used to respond to DoA and to follow nutrient gradients. Moreover, these genes were not significantly changed by OA or PFD_oA at any point in the time course, suggesting a specific response to PFOA at 48 h. Furthermore, genes encoding autoinducer-2 (AI-2), *luxS*, a quorum sensing (QS) molecule [131] and the ABC transporter *lsr* operon, used for AI-2 uptake, were significantly upregulated by PFOA at 48 h (Fig. 8D; Table SI 14). AI-2 controls gene expression of chemotaxis and flagellar assembly and has a possible link to biofilm formation [132]. A previous study found PFAS induced the production of EPS, biofilm precursor, in *Rhodococcus* as a stress response [133]. Although EPS biosynthesis genes are downregulated at 48 h, with the exception of the *rfb* operon (Table SI 14), additional measurements after 48 h could provide insight into possible PFOA-induced biofilm formation.

Conclusions

In summary, we performed time course RNA-seq to characterize the transcriptional responses of mid-exponential phase and stationary phase *E. coli* to PFCAs, PFOA and PFD_oA. Our results suggest 100 μmol/L of either PFCa or respective NFCAs do not statistically impact the growth of *E. coli* at any point in the time course relative to the untreated control. However, differential expression analysis revealed PFOA and PFD_oA did induce statistically significant changes in gene expression of the formate regulon and sulfate assimilation at mid-exponential phase and ferrous iron transport, the molecular chaperone network, and motility processes during stationary phase. The time course enabled us to capture the specific and common responses of *E. coli* to PFCAs and NFCAs across time and helped to characterize responses that were specific to a single growth phase or prolonged over

time. For instance, our results indicate a requirement for sulfur-containing compounds, like cysteine, during mid-exponential phase as sulfate assimilation components were overexpressed in response specifically to PFDoA. In contrast, overexpression of ferrous iron transporters and amino acid enzymes by PFOA and PFDoA early in stationary phase suggest a time dependent need for ferrous iron and select amino acids. Although differentially expressed at different phases within the time course, sulfur-containing compounds and iron participate in various redox reactions within the cell which could suggest PFCA induce adjustments to cellular redox. Interestingly, PFOA induced the largest change in gene expression of this study at 48h, whereas PFDoA induced a minor change in expression. These results suggest different modes of interactions between *E. coli* and two PFCA that only differ in length by four carbons but have different physiochemical properties.

These results not only provide additional biological context of the response of *E. coli* to PFCA at key phases of growth, but possible novel engineering targets to facilitate the development of future environmental monitoring and mitigation strategies. For example, gene expression of numerous small regulatory RNAs and their targets was only significantly changed by PFCA and not by NFCA (Fig. 7C), suggesting a unique response to fluorinated compounds that could be utilized in a whole cell biosensor. Additionally, the moderate upregulation of *crcB*, a putative fluoride exporter downstream of a fluoride riboswitch, by PFOA at 48 h (Fig. 8A), suggests there may have been some removal of fluorine from the PFOA over the time course, warranting further investigation as a mitigation strategy.

Even though these measurements offer a comprehensive transcriptomic snapshot of the relationship between PFCA and a model bacterium at key growth phases, further characterization efforts would benefit from additional measurements of PFAS with different molecular structures, concentrations, and complex mixtures to explore the extent to which the responses identified here are conserved and identify novel responses. While significant changes in gene expression were induced at the concentration studied here, no obvious growth defects were observed, suggesting *E. coli* is relatively tolerant of PFAS compared to eukaryotes [36–39]. These results are in line with recent studies showing multiple enteric bacteria can grow uninhibited with up to 500 $\mu\text{mol/L}$ of PFAS [35]. Conducting similar studies on environmental microorganisms and microbial communities could provide insight into conserved responses across genera and species and how contamination by PFAS impacts the environment. As technology continues to advance, improved gene expression measurements at the single cell, population, and community level combined with

multiomics level analysis would enable more accurate, impactful understanding of PFAS at all levels of biology. This complete picture could aid in the rapid development of inexpensive and easy-to-deploy living measurement systems for in situ environmental monitoring and mitigation strategies.

Materials and methods

Bacterial strain

Escherichia coli MG1655 ATCC 47076 was obtained from the American Type Culture Collection (ATCC). The strain was maintained on Luria-Bertani (LB) agar plates at 37 °C prior to use.

PFOA, PFDoA, and NFCA Preparation

Two PFCA, perfluorooctanoic acid (96%, PFOA) and tricosafuorododecanoic acid (95%, perfluorododecanoic acid, PFDoA) were used in this study. See Table SI 15 for additional chemical stock information. PFOA and PFDoA were dissolved in dimethyl sulfoxide (DMSO) to prepare a stock solution of 100 mmol/L. Concentrations in the growth medium for growth experiments were 100 $\mu\text{mol/L}$ and 10 $\mu\text{mol/L}$. The final concentration in the growth medium for sequencing experiments was 100 $\mu\text{mol/L}$. DMSO was present in the growth medium at a final volume fraction of 0.1%. Dodecanoic acid (98%, DoA) was prepared in the same way as the PFCA stocks. Octanoic acid (99%, OA) samples contained an addition of DMSO to the growth medium. All untreated samples contained an equivalent concentration of DMSO and were devoid of PFCA addition.

E. coli growth in PFCA or NFCA containing medium

E. coli MG1655 was struck onto an LB agar (BD Difco) plate from a glycerol stock obtained from ATCC. Overnight cultures for each biological replicate were prepared by inoculating 3 mL of M9 minimal medium [134], without PFCA or NFCA addition, with an individual colony incubated at 37 °C, 250 rpm (Table SI 15). For flask-based growth experiments, PFCA stocks, NFCA stocks, or DMSO were added into M9 prior inoculation with *E. coli* cultures as described above. To prepare sample flasks, 50 mL of M9 in sterile 125 mL baffled flasks was inoculated with overnight culture and adjusted to a starting optical density at 600 nm of 0.01 (SI Fig. 1; Table SI 1). Cultures were incubated at 37 °C, 250 rpm for 48 h. Independent biological triplicate flasks were used for each PFCA, NFCA, and untreated control group.

To obtain the optical density of each culture, bacterial growth was monitored in each culture with absorbance measurements at 600 nm in technical triplicate throughout the 48 h period. A Biotek Epoch2 microplate reader was used for absorbance measurements. A two-way mixed ANOVA of optical density measurements

and time was performed in RStudio running R version 4.2.2 with functions from packages tidyverse (v2.0.0) and rstatix (v0.7.2) [135, 136]. See SI Note 1. A mixed ANOVA was used because the dependent variable (optical density) was subjected to both a between-subjects variable (PFCA or NFCA) and a within-subjects variable (time).

Total RNA extraction, cDNA library preparation, and RNA sequencing

Cell pellets of *E. coli* from each sample type (PFCA, NFCA, or untreated control) were harvested at 6 h, 24 h, and 48 h and normalized to an OD₆₀₀ of 1.0. Samples were spun down at 5,500xg for 7 min at 4 °C, and supernatant was removed prior to storage at -80 °C until total RNA extraction.

Total RNA was extracted from biological triplicates of each PFCA, NFCA, and untreated control at 6 h, 24 h, and 48 h using RNeasy Mini Kit (Qiagen) according to the manufacturer's instructions with an on-column DNase I digestion for 15 min using an RNase-free DNase Set (Qiagen). Cells were lysed in 200 µL Tris-EDTA buffer solution, pH 8.0 containing 20 g/L lysozyme (Sigma Aldrich) at room temperature for 10 min with vortexing every 2 min. RNA was eluted in 35 µL of molecular grade water (Invitrogen) and stored at -80 °C. The concentration and purity of total RNA were quantified on a Qubit 4 fluorometer (Invitrogen) using Qubit RNA Broad Range Assay Kit, DeNovix D-11 Series Spectrophotometer, and 4200 TapeStation System (Agilent) using RNA Screen-Tape Analysis.

Total RNA samples were sent to Azenta Life Sciences (USA) for cDNA library preparation using TruSeq Stranded mRNA kit (Illumina) and next-generation sequencing (Strand-Specific RNA-Seq Service) using an Illumina HiSeq platform for 2 × 150 bp paired-end reads. Average sequencing depth obtained was 7.81 million. Additional information on sequencing is provided in (Table SI 2).

Bioinformatic analysis

Bioinformatic analysis was performed on an Amazon Web Service EC2 instance and locally on RStudio. TrimGalore (v0.6.7) with Cutadapt (v3.5) and fastQC (v0.11.9) was used to remove adapter sequences and low-quality reads from each raw read file [137–139]. HISAT2 (v2.2.1) [140] was used to align paired-end reads to *E. coli* MG1655 reference genome (GenBank accession GCA_000005845.2). Alignment scores and quality metric scores are shown in Table SI 2. Samtools (v1.13) was used for file conversion of SAM files to sorted BAM files before transcript assembly was performed with Stringtie (v2.2.1) [141, 142]. In RStudio running R version 4.2.2, tximport (v1.26.1) prepared count tables

from Stringtie transcript-level estimates [135, 136, 143]. DESeq2 (v1.38.3) was used to perform differential gene expression analysis with a negative binomial distribution model [50]. The time specific untreated control served as the control baseline for all pairwise comparisons. In this study, we consider genes to be differentially expressed if the Benjamini-Hochberg adjusted p-value (padj) is less than 0.05. We mark moderate and significant differential expression with absolute values of the log₂ fold change greater than or equal to 1.2 and 1.5, respectively. Gene ontology and Kyoto Encyclopedia of Genes and Genomes pathway over-representation analyses were performed using clusterProfiler (v4.6.2) using the *E. coli* K12 organism package, org.EcK12.eg.db, (v3.19.1) and KEGG organism eco [144, 145] (SI File 1). Additional data curation was performed using EcoCyc [146].

Abbreviations

PFAS	Per- and polyfluoroalkyl substances
PFOA	Perfluorooctanoic acid
PFD ₁₂ OA	Perfluorododecanoic acid
NFCA	Non-fluorinated carboxylic acids
USEPA	U. S. Environmental Protection Agency
OECD	Organization of Economic Co-operation and Development
LC-MS	Liquid chromatography – mass spectrometry
RNA-seq	RNA sequencing
DMSO	Dimethyl sulfoxide
OA	Octanoic acid
DoA	Dodecanoic acid
OD ₆₀₀	Optical density at 600 nm
NGS	Next generation sequencing
PCA	Principal component analysis
NAD	Nicotinamide adenine dinucleotide
FHL	Formate hydrogenlyase
ABC	ATP-binding cassette
APS	Adenosine 5'-phosphosulfate
Fe ²⁺	Ferrous iron
Fe ³⁺	Ferric iron
sRNA	Small regulatory RNA
TCA	The citric acid cycle
PEP	Phosphoenolpyruvate
TF	Trigger factor
RNAP	RNA polymerase
Psp	Phage-shock-protein
LPS	Lipopolysaccharide
EPS	Extracellular polysaccharide
AI-2	Autoinducer-2
QS	Quorum sensing

Supplementary Information

The online version contains supplementary material available at <https://doi.org/10.1186/s12864-025-12109-4>.

Supplementary Material 1.
Supplementary Material 2.
Supplementary Material 3.
Supplementary Material 4.
Supplementary Material 5.

Acknowledgements

The authors would like to thank Elizabeth Strychalski, Allison Yaguchi, Justin Wagner, Svetlana Ikononova, and Zoila Jurado Quiroga for insightful

discussions throughout the project and on the manuscript. Figures 1 and 5, SI Figure 1, and SI Figure 6 were created with BioRender.com.

Authors' contributions

M.E.W. conceived the project, designed experiments, conducted data analysis, and wrote the first draft with input from S.W.S. O.B.V. designed growth experiments. M.E.W. and S.W.S. edited the manuscript with input from all authors.

Funding

This work was supported by a National Research Council Postdoctoral Fellowship to M.E.W.

Data availability

The data presented in this study have been deposited in the National Center for Biotechnology Information's Gene Expression Omnibus (146) and are accessible through GEO Series accession number GSE288896 (<https://www.ncbi.nlm.nih.gov/geo/query/acc.cgi?acc=GSE288896>).

Declarations

Ethics approval and consent to participate

Not applicable.

Consent for publication

Not applicable.

Competing interests

The authors declare no competing interests.

Disclaimer

Certain commercial entities, equipment, or materials may be identified in this document to describe an experimental procedure or concept adequately. Such identification is not intended to imply recommendation or endorsement by the National Institute of Standards and Technology, nor is it intended to imply that the entities, materials, or equipment are necessarily the best available for the purpose. Official contribution of the National Institute of Standards and Technology; not subject to copyright in the United States.

Author details

¹Material Measurement Laboratory, National Institute of Standards and Technology, Department of Commerce, Gaithersburg, MD, USA

Received: 4 March 2025 / Accepted: 10 September 2025

Published online: 07 November 2025

References

- Parsons JR, Sáez M, Dolfig J, de Voogt P. Biodegradation of perfluorinated compounds. *Rev Environ Contam Toxicol*. 2008;196:53–71.
- Glüge J, Scheringer M, Cousins IT, DeWitt JC, Goldenman G, Herzke D, et al. An overview of the uses of per- and polyfluoroalkyl substances (PFAS). *Environ Sci Process Impacts*. 2020;22(12):2345–73.
- Williams AJ, Gaines LGT, Grulke CM, Lowe CN, Sinclair GFB, Samano V, et al. Assembly and curation of lists of Per- and polyfluoroalkyl substances (PFAS) to support environmental science research. *Front Environ Sci*. 2022;10:1–13.
- Faust JA. PFAS on atmospheric aerosol particles: a review. *Environ Sci Process Impacts*. 2023;25(2):133–50.
- Abunada Z, Alazaiza MYD, Bashir MJK. An overview of per- and polyfluoroalkyl substances (PFAS) in the environment: source, fate, risk and regulations. *Water*. 2020;12:12(3590). <https://doi.org/10.3390/w12123590>.
- LaKind JS, Naiman J, Verner MA, Lévêque L, Fenton S. Per- and polyfluoroalkyl substances (PFAS) in breast milk and infant formula: a global issue. *Environ Res*. 2023;219:115042.
- Graber JM, Alexander C, Laumbach RJ, Black K, Strickland PO, Georgopoulos PG, et al. Per and polyfluoroalkyl substances (PFAS) blood levels after contamination of a community water supply and comparison with 2013–2014 NHANES. *J Expo Sci Environ Epidemiol*. 2019;29(2):172–82.
- Li J, Sun J, Li P. Exposure routes, bioaccumulation and toxic effects of per- and polyfluoroalkyl substances (PFAS) on plants: a critical review. *Environ Int*. 2022;158:106891.
- Piva E, Giorgetti A, Ioime P, Morini L, Freni F, Faro FL, et al. Hair determination of per- and polyfluoroalkyl substances (PFAS) in the Italian population. *Toxicology*. 2021;458:152849.
- Brusseau ML, Anderson RH, Guo B. PFAS concentrations in soils: background levels versus contaminated sites. *Sci Total Environ*. 2020;740:140017.
- Coperchini F, Croce L, Ricci G, Magri F, Rotondi M, Imbriani M, et al. Thyroid disrupting effects of old and new generation PFAS. *Front Endocrinol (Lausanne)*. 2020;11:612320.
- Evich MG, Davis MJB, McCord JP, Acrey B, Awkerman JA, Knappe DRU, et al. Per- and polyfluoroalkyl substances in the environment. *Science*. 2022;375(6580):eabg9065.
- Zhang X, Zhao L, Ducatman A, Deng C, von Stackelberg KE, Danford CJ. Association of per- and polyfluoroalkyl substance exposure with fatty liver disease risk in US adults. *JHEP Reports*. 2023;5(5):100694.
- Khan EA, Zhang X, Hanna EM, Yadette F, Jonassen I, Goksøyr A, et al. Application of quantitative transcriptomics in evaluating the ex vivo effects of per- and polyfluoroalkyl substances on Atlantic Cod (*Gadus morhua*) ovarian physiology. *Sci Total Environ*. 2021;755(Pt 1):142904.
- CompTox chemicals dashboard, PFAS master list of PFAS substances [Internet]. 2022. Available from: <https://comptox.epa.gov/dashboard/chemical-lists/PFASMASTER>
- OECD H. Reconciling terminology of the universe of per-and polyfluoroalkyl substances: recommendations and practical guidance. OECD Publishing Paris; 2021. p. 45.
- Buck RC, Franklin J, Berger U, Conder JM, Cousins IT, de Voogt P, et al. Per-fluoroalkyl and polyfluoroalkyl substances in the environment: terminology, classification, and origins. *Integr Environ Assess Manag*. 2011;7(4):513–41.
- Berhanu A, Mutanda I, Taolin J, Qaria MA, Yang B, Zhu D. A review of microbial degradation of per- and polyfluoroalkyl substances (PFAS): biotransformation routes and enzymes. *Sci Total Environ*. 2023;859(Pt 1):160010.
- Weiner B, Yeung LWY, Marchington EB, D'Agostino LA, Mabury SA. Organic fluorine content in aqueous film forming foams (AFFFs) and biodegradation of the foam component 6: 2 fluorotelomermercaptoalkylamido sulfonate (6: 2 FTSA). *Environ Chem*. 2013;10(6):486–93.
- Gonda N, Zhang C, Tepedelen D, Smith A, Schaefer C, Higgins CP. Quantitative assessment of poly- and perfluoroalkyl substances (PFASs) in aqueous film forming foam (AFFF)-impacted soils: a comparison of analytical protocols. *Anal Bioanal Chem*. 2024. <https://doi.org/10.1007/s00216-024-05585-2>.
- Lopez-Vazquez J, Montes R, Rodil R, Cela R, Martinez-Pontevedra JA, Pena MT et al. Determination of regulated perfluoroalkyl substances (PFAS) in drinking water according to directive 2020/2184/EU. *Environ Sci Pollut Res Int*. 2024. <https://doi.org/10.1007/s11356-024-34852-z>
- USEPA. PFAS Analytical Methods Development and Sampling Research. 2024 [Available from: <https://www.epa.gov/water-research/pfas-analytical-methods-development-and-sampling-research>
- Malouchi N, Chatzimichailidou S, Tolkou AK, Kyzas GZ, Calgario L, Marcomini A, et al. The removal of per- and poly-fluoroalkyl substances from water: a review on destructive and non-destructive methods. *Separations*. 2024;11(4):122.
- Mahinroosta R, Senevirathna L. A review of the emerging treatment technologies for PFAS contaminated soils. *J Environ Manage*. 2020;255:109896.
- Stockbridge RB, Wackett LP. The link between ancient microbial fluoride resistance mechanisms and bioengineering organofluorine degradation or synthesis. *Nat Commun*. 2024;15(1):4593.
- Cordner A, Goldenman G, Birnbaum LS, Brown P, Miller MF, Mueller R, et al. The true cost of PFAS and the benefits of acting now. *Environ Sci Technol*. 2021;55(14):9630–3.
- Sharma N, Kumar V, Sugumar V, Umesh M, Sondhi S, Chakraborty P, et al. A comprehensive review on the need for integrated strategies and process modifications for per- and polyfluoroalkyl substances (PFAS) removal: current insights and future prospects. *Case Stud Chem Environ Eng*. 2024;9:100623.
- Mann MM, Berger BW. A genetically-encoded biosensor for direct detection of perfluorooctanoic acid. *Sci Rep*. 2023;13(1):15186.
- Thompson D, Zolfigol N, Xia Z, Lei Y. Recent progress in per- and polyfluoroalkyl substances (PFAS) sensing: a critical mini-review. *Sens Actuators Rep*. 2024;7:100189.
- Tang Z, Vogel TM, Wang Q, Wei C, Ali M, Song X. Microbial defluorination of TFA, PFOA, and HFPO-DA by a native microbial consortium under anoxic conditions. *J Hazard Mater*. 2024;465:133217.

31. Griebler C, Lueders T. Microbial biodiversity in groundwater ecosystems. *Freshw Biol.* 2009;54(4):649–77.
32. Jagevall S, Rabe L, Pedersen K. Abundance and diversity of biofilms in natural and artificial aquifers of the Aspö hard rock laboratory, Sweden. *Microb Ecol.* 2011;61(2):410–22.
33. Nguyen J, Lara-Gutiérrez J, Stocker R. Environmental fluctuations and their effects on microbial communities, populations and individuals. *FEMS Microbiol Rev.* 2021. <https://doi.org/10.1093/femsre/fuaa068>.
34. Norman TM, Lord ND, Paulsson J, Losick R. Stochastic switching of cell fate in microbes. *Annu Rev Microbiol.* 2015;69:381–403.
35. Lindell AE, Griesshammer A, Michaelis L, Papagiannidis D, Ochner H, Kamrad S, et al. Human gut bacteria bioaccumulate per- and polyfluoroalkyl substances. *Nat Microbiol.* 2025;10(7):1630–47.
36. Beale DJ, Sinclair GM, Shah R, Paten AM, Kumar A, Long SM, et al. A review of omics-based PFAS exposure studies reveals common biochemical response pathways. *Sci Total Environ.* 2022;845:157255.
37. Reardon AJF, Rowan-Carroll A, Ferguson SS, Leingartner K, Gagne R, Kuo B, et al. Potency ranking of per- and polyfluoroalkyl substances using high-throughput transcriptomic analysis of human liver spheroids. *Toxicol Sci.* 2021;184(1):154–69.
38. Rericha Y, St Mary L, Truong L, McClure R, Martin JK, Leonard SW, et al. Diverse PFAS produce unique transcriptomic changes linked to developmental toxicity in zebrafish. *Front Toxicol.* 2024;6:1425537.
39. Yang M, Ye J, Qin H, Long Y, Li Y. Influence of perfluorooctanoic acid on proteomic expression and cell membrane fatty acid of *Escherichia coli*. *Environ Pollut.* 2017;220(Pt A):532–9.
40. Bhatia RP, Kirit HA, Predeus AV, Bollback JP. Transcriptomic profiling of *Escherichia coli* K-12 in response to a compendium of stressors. *Sci Rep.* 2022;12(1):8788.
41. Wintenberg M, Manglass L, Martinez NE, Blenner M. Global transcriptional response of *Escherichia coli* exposed in situ to different low-dose ionizing radiation sources. *mSystems.* 2023;8(2):e0071822.
42. Valat C, Hirchaud E, Drapeau A, Touzain F, de Boisseson C, Haenni M, et al. Overall changes in the transcriptome of *Escherichia coli* O26:H11 induced by a subinhibitory concentration of ciprofloxacin. *J Appl Microbiol.* 2020;129(6):1577–88.
43. Spiteri D, Griffin S, Karatzas KA, Scerri C, Valdramidis VP. *Escherichia coli* K-12 transcriptomics for assessing the mechanism of action of high-power ultrasound. *Microorganisms.* 2023. <https://doi.org/10.3390/microorganisms11112768>.
44. Zango ZU, Ethiraj B, Al-Mubaddel FS, Alam MM, Lawal MA, Kadir HA, et al. An overview on human exposure, toxicity, solid-phase Microextraction and adsorptive removal of perfluoroalkyl carboxylic acids (PFCA) from water matrices. *Environ Res.* 2023;231(Pt 2):116102.
45. Addicks GC, Rowan-Carroll A, Reardon AJF, Leingartner K, Williams A, Meier MJ, et al. Per- and polyfluoroalkyl substances (PFAS) in mixtures show additive effects on transcriptomic points of departure in human liver spheroids. *Toxicol Sci.* 2023;194(1):38–52.
46. Ji C, Stockbridge RB, Miller C. Bacterial fluoride resistance, Flu channels, and the weak acid accumulation effect. *J Gen Physiol.* 2014;144(3):257–61.
47. Adamek E, Pawłowska-Góral K, Bober K. In vitro and in vivo effects of fluoride ions on enzyme activity. *Ann Acad Med Stetin.* 2005;51(2):69–85.
48. Breaker RR. New insight on the response of bacteria to fluoride. *Caries Res.* 2012;46(1):78–81.
49. Ishihama A. Adaptation of gene expression in stationary phase bacteria. *Curr Opin Genet Dev.* 1997;7(5):582–8.
50. Love MI, Huber W, Anders S. Moderated estimation of fold change and dispersion for RNA-seq data with DESeq2. *Genome Biol.* 2014;15(12):550.
51. Nobelmann B, Lengeler JW. Molecular analysis of the Gat genes from *Escherichia coli* and of their roles in galactitol transport and metabolism. *J Bacteriol.* 1996;178(23):6790–5.
52. Ehrmann M, Boos W, Ormseth E, Schweizer H, Larson TJ. Divergent transcription of the sn-glycerol-3-phosphate active transport (glpT) and anaerobic sn-glycerol-3-phosphate dehydrogenase (glpA GlpC glpB) genes of *Escherichia coli* K-12. *J Bacteriol.* 1987;169(2):526–32.
53. Gerike U, Hough DW, Russell NJ, Dyal-Smith ML, Danson MJ. Citrate synthase and 2-methylcitrate synthase: structural, functional and evolutionary relationships. *Microbiology.* 1998;144(Pt 4):929–35.
54. Yamanaka Y, Oshima T, Ishihama A, Yamamoto K. Characterization of the YdeO regulon in *Escherichia coli*. *PLoS ONE.* 2014;9(11):e111962.
55. Navarro Llorens JM, Tormo A, Martínez-García E. Stationary phase in gram-negative bacteria. *FEMS Microbiol Rev.* 2010;34(4):476–95.
56. Ollagnier-de Choudens S, Loiseau L, Sanakis Y, Barras F, Fontecave M. Quinolinate synthetase, an iron-sulfur enzyme in NAD biosynthesis. *FEBS Lett.* 2005;579(17):3737–43.
57. Skibinski DA, Golby P, Chang YS, Sargent F, Hoffman R, Harper R, et al. Regulation of the hydrogenase-4 Operon of *Escherichia coli* by the sigma(54)-dependent transcriptional activators FhIA and hyfR. *J Bacteriol.* 2002;184(23):6642–53.
58. Pinske C, Sargent F. Exploring the directionality of *Escherichia coli* formate hydrogenlyase: a membrane-bound enzyme capable of fixing carbon dioxide to organic acid. *Microbiol Open.* 2016;5(5):721–37.
59. McDowall JS, Murphy BJ, Haumann M, Palmer T, Armstrong FA, Sargent F. Bacterial formate hydrogenlyase complex. *Proc Natl Acad Sci U S A.* 2014;111(38):E3948–56.
60. Lutz S, Jacobi A, Schlensog V, Böhm R, Sawers G, Böck A. Molecular characterization of an operon (hyp) necessary for the activity of the three hydrogenase isoenzymes in *Escherichia coli*. *Mol Microbiol.* 1991;5(1):123–35.
61. Pao SS, Paulsen IT, Saier MH. Major facilitator superfamily. *Microbiol Mol Biol Rev.* 1998;62(1):1–34.
62. Saier MH, Reddy VS, Moreno-Hagelsieb G, Hendargo KJ, Zhang Y, Iddamsetty V, et al. The transporter classification database (TCDB): 2021 update. *Nucleic Acids Res.* 2021;49(D1):D461–7.
63. Tanaka Y, Yoshikawa K, Takeuchi A, Ichikawa M, Mori T, Uchino S, et al. Crystal structure of a yeeE/yede family protein engaged in thiosulfate uptake. *Sci Adv.* 2020;6(35):eaba7637.
64. Sirko A, Hryniewicz M, Hulanicka D, Böck A. Sulfate and thiosulfate transport in *Escherichia coli* K-12: nucleotide sequence and expression of the cystwam gene cluster. *J Bacteriol.* 1990;172(6):3351–7.
65. Imlay KRC, Korshunov S, Imlay JA. Physiological roles and adverse effects of the two cystine importers of *Escherichia coli*. *J Bacteriol.* 2015;197(23):3629–44.
66. Ikei M, Miyazaki R, Monden K, Naito Y, Takeuchi A, Takahashi YS, et al. YeeD is an essential partner for YeeE-mediated thiosulfate uptake in bacteria and regulates thiosulfate ion decomposition. *PLoS Biol.* 2024;22(4):e3002601.
67. Leyh TS, Vogt TF, Suo Y. The DNA sequence of the sulfate activation locus from *Escherichia coli* K-12. *J Biol Chem.* 1992;267(15):10405–10.
68. Leyh TS, Taylor JC, Markham GD. The sulfate activation locus of *Escherichia coli* K12: cloning, genetic, and enzymatic characterization. *J Biol Chem.* 1988;263(5):2409–16.
69. Deutch CE, Spahija I, Wagner CE. Susceptibility of *Escherichia coli* to the toxic L-proline analogue L-selenaproline is dependent on two L-cystine transport systems. *J Appl Microbiol.* 2014;117(5):1487–99.
70. Kredich NM. The molecular basis for positive regulation of Cys promoters in *Salmonella typhimurium* and *Escherichia coli*. *Mol Microbiol.* 1992;6(19):2747–53.
71. Andrews SC, Robinson AK, Rodriguez-Quinones F. Bacterial iron homeostasis. *FEMS Microbiol Rev.* 2003;27(2–3):215–37.
72. McHugh JP, Rodriguez-Quinones F, Abdul-Tehrani H, Svistunenko DA, Poole RK, Cooper CE, et al. Global iron-dependent gene regulation in *Escherichia coli*. A new mechanism for iron homeostasis. *J Biol Chem.* 2003;278(32):29478–86.
73. Hantke K. Is the bacterial ferrous iron transporter FeoB a living fossil? *Trends Microbiol.* 2003;11(5):192–5.
74. Kammler M, Schön C, Hantke K. Characterization of the ferrous iron uptake system of *Escherichia coli*. *J Bacteriol.* 1993;175(19):6212–9.
75. Lau CK, Ishida H, Liu Z, Vogel HJ. Solution structure of *Escherichia coli* FeoA and its potential role in bacterial ferrous iron transport. *J Bacteriol.* 2013;195(1):46–55.
76. Massé E, Salvail H, Desnoyers G, Arguin M. Small RNAs controlling iron metabolism. *Curr Opin Microbiol.* 2007;10(2):140–5.
77. Balbontin R, Villagra N, Pardos de la Gándara M, Mora G, Figueroa-Bossi N, Bossi L. Expression of iron, the Salmochelin siderophore receptor, requires mRNA activation by RyhB small RNA homologues. *Mol Microbiol.* 2016;100(1):139–55.
78. Johnston NR, Strobel SA. Principles of fluoride toxicity and the cellular response: a review. *Arch Toxicol.* 2020;94(4):1051–69.
79. Murashko ON, Yeh KH, Yu CA, Kabardin VR, Lin-Chao S. Sodium fluoride exposure leads to ATP depletion and altered RNA decay in *Escherichia coli* under anaerobic conditions. *Microbiol Spectr.* 2023;11(2):e0415822.
80. Ratledge C. Iron, mycobacteria and tuberculosis. *Tuberculosis (Edinb).* 2004;84(1–2):110–30.
81. Tsylyents U, Burmistrz M, Wojciechowska M, Stępień J, Maj P, Trylska J. Iron uptake pathway of. *Front Microbiol.* 2024;15:1331021.

82. Postle K, Larsen RA. TonB-dependent energy transduction between outer and cytoplasmic membranes. *Biometals*. 2007;20(3–4):453–65.
83. Grosse C, Scherer J, Koch D, Otto M, Taudte N, Grass G. A new ferrous iron-uptake transporter, EfeU (YcdN), from *Escherichia coli*. *Mol Microbiol*. 2006;62(1):120–31.
84. Clarke TA, Dennison V, Seward HE, Burlat B, Cole JA, Hemmings AM, et al. Purification and spectropotentiometric characterization of *Escherichia coli* nrfb, a decaheme homodimer that transfers electrons to the decaheme periplasmic nitrite reductase complex. *J Biol Chem*. 2004;279(40):41333–9.
85. Kranz RG, Richard-Fogal C, Taylor JS, Frawley ER. Cytochrome c biogenesis: mechanisms for covalent modifications and trafficking of Heme and for Heme-iron redox control. *Microbiol Mol Biol Rev*. 2009;73(3):510–28. Table of Contents.
86. Baez A, Sharma AK, Bryukhanov A, Anderson ED, Olivares-Hernández R, et al. Iron availability enhances the cellular energetics of aerobic *Escherichia coli* cultures while upregulating anaerobic respiratory chains. *New Biotechnol*. 2022;71:11–20.
87. Erickson DW, Schink SJ, Patsalo V, Williamson JR, Gerland U, Hwa T. A global resource allocation strategy governs growth transition kinetics of *Escherichia coli*. *Nature*. 2017;551(7678):119–23.
88. Jozefczuk S, Klie S, Catchpole G, Szymanski J, Cuadros-Inostroza A, Steinhauser D, et al. Metabolomic and transcriptomic stress response of *Escherichia coli*. *Mol Syst Biol*. 2010;6:364.
89. Ren X, Wei Y, Zhao H, Shao J, Zeng F, Wang Z, et al. A comprehensive review and comparison of L-tryptophan biosynthesis in *Saccharomyces cerevisiae* and *Escherichia coli*. *Front Bioeng Biotechnol*. 2023;11:1261832.
90. Santillan M, Zeron ES. Dynamic influence of feedback enzyme inhibition and transcription attenuation on the tryptophan operon response to nutritional shifts. *J Theor Biol*. 2004;231(2):287–98.
91. Hao R, Wang S, Jin X, Yang X, Qi Q, Liang Q. Dynamic and balanced regulation of the *thrABC* operon gene for efficient synthesis of L-threonine. *Front Bioeng Biotechnol*. 2023;11:118948.
92. Wechsler JA, Adelberg EA. Antipolarity in the *llv* operon of *Escherichia coli* K-12. *J Bacteriol*. 1969;98(3):1179–94.
93. Ponath F, Hor J, Vogel J. An overview of gene regulation in bacteria by small RNAs derived from mRNA 3' ends. *FEMS Microbiol Rev*. 2022. <https://doi.org/10.1093/femsre/fuac017>.
94. Holmqvist E, Vogel J. RNA-binding proteins in bacteria. *Nat Rev Microbiol*. 2018;16(10):601–15.
95. Hor J, Matera G, Vogel J, Gottesman S, Storz G. Trans-acting small RNAs and their effects on gene expression in *Escherichia coli* and *Salmonella enterica*. *EcoSal Plus*. 2020. <https://doi.org/10.1128/ecosalplus.esp-0030-2019>.
96. Fitzgerald NJM, Simcik MF, Novak PJ. Perfluoroalkyl substances increase the membrane permeability and quorum sensing response in *Aliivibrio fischeri*. *Environ Sci Technol Lett*. 2018;5(1):26–31.
97. Fitzgerald NJM, Wargenau A, Sorenson C, Pedersen J, Tufenkji N, Novak PJ, et al. Partitioning and accumulation of perfluoroalkyl substances in model lipid bilayers and bacteria. *Environ Sci Technol*. 2018;52(18):10433–40.
98. McIlwain BC, Ruprecht MT, Stockbridge RB. Membrane exporters of fluoride ion. *Annu Rev Biochem*. 2021;90:559–79.
99. Stockbridge RB, Robertson JL, Kolmakova-Partensky L, Miller C. A family of fluoride-specific ion channels with dual-topology architecture. *Elife*. 2013;2:e01084.
100. Qin J, Chai G, Brewer JM, Lovelace LL, Lebioda L. Fluoride inhibition of enolase: crystal structure and thermodynamics. *Biochemistry*. 2006;45(3):793–800.
101. McCormick NE, Jakeman DL. On the mechanism of phosphoenolpyruvate synthetase (PEPs) and its inhibition by sodium fluoride: potential magnesium and aluminum fluoride complexes of phosphoryl transfer. *Biochem Cell Biol*. 2015;93(3):236–40.
102. Zhou H, Zhang Y, Long CP, Xia X, Xue Y, Ma Y, et al. A citric acid cycle-deficient *Escherichia coli* as an efficient chassis for aerobic fermentations. *Nat Commun*. 2024;15(1):2372.
103. Yu BJ, Sung BH, Lee JY, Son SH, Kim MS, Kim SC. SucAB and SucCD are mutually essential genes in *Escherichia coli*. *FEMS Microbiol Lett*. 2006;254(2):245–50.
104. Förster AH, Gescher J. Metabolic engineering of *Escherichia coli* for production of mixed-acid fermentation end products. *Front Bioeng Biotechnol*. 2014;2:16.
105. Nikolaeva DD, Gelfand MS, Garushyants SK. Simplification of ribosomes in bacteria with tiny genomes. *Mol Biol Evol*. 2021;38(1):58–66.
106. Njenga R, Boele J, Öztürk Y, Koch H. Coping with stress: how bacteria fine-tune protein synthesis and protein transport. *J Biol Chem*. 2023. <https://doi.org/10.1016/j.jbc.2023.105163>.
107. Marquis RE. Antimicrobial actions of fluoride for oral bacteria. *Can J Microbiol*. 1995;41(11):955–64.
108. Goldberg AL, Moerschell RP, Chung CH, Maurizi MR. ATP-dependent protease La (Lon) from *Escherichia coli*. *Methods Enzymol*. 1994;244:350–75.
109. Lee I, Suzuki CK. Functional mechanics of the ATP-dependent Lon protease-lessons from endogenous protein and synthetic peptide substrates. *Biochim Biophys Acta*. 2008;1784(5):727–35.
110. Luo S, McNeill M, Myers TG, Hohman RJ, Levine RL. Lon protease promotes survival of *Escherichia coli* during anaerobic glucose starvation. *Arch Microbiol*. 2008;189(2):181–5.
111. Kuroda A, Nomura K, Ohtomo R, Kato J, Ikeda T, Takiguchi N, et al. Role of inorganic polyphosphate in promoting ribosomal protein degradation by the Lon protease in *E. coli*. *Science*. 2001;293(5530):705–8.
112. Wilkens S. Structure and mechanism of ABC transporters. *F1000Prime Rep*. 2015;7:14.
113. de Keyzer J, van der Does C, Driessen AJ. The bacterial translocase: a dynamic protein channel complex. *Cell Mol Life Sci*. 2003;60(10):2034–52.
114. Sanganna Gari R R, Chattrakun K, Marsh B P, Mao C, Chada N, Randall L L, et al. Direct visualization of the *E. coli* sec translocase engaging precursor proteins in lipid bilayers. *Sci Adv*. 2019;5(6):eaav9404.
115. Chatzi KE, Sardis MF, Economou A, Karamanou S. SecA-mediated targeting and translocation of secretory proteins. *Biochim Biophys Acta*. 2014;1843(8):1466–74.
116. Natale P, Bruser T, Driessen AJ. Sec- and Tat-mediated protein secretion across the bacterial cytoplasmic membrane—distinct translocases and mechanisms. *Biochim Biophys Acta*. 2008;1778(9):1735–56.
117. Saibil H. Chaperone machines for protein folding, unfolding and disaggregation. *Nat Rev Mol Cell Biol*. 2013;14(10):630–42.
118. Bukau B, Walker GC. Cellular defects caused by deletion of the *Escherichia coli* DnaK gene indicate roles for heat shock protein in normal metabolism. *J Bacteriol*. 1989;171(5):2337–46.
119. Storey JM, Storey KB. Chaperone proteins: universal roles in surviving environmental stress. *Cell Stress Chaperones*. 2023;28(5):455–66.
120. Yadav A, Vuković L, Narayan M. An atomic and molecular insight into how PFOA reduces α -helicity, compromises substrate binding, and creates binding pockets in a model globular protein. *J Am Chem Soc*. 2024;146(18):12766–77.
121. Xu M, Cui Z, Zhao L, Hu S, Zong W, Liu R. Characterizing the binding interactions of PFOA and PFOS with catalase at the molecular level. *Chemosphere*. 2018;203:360–7.
122. Sutherland C, Murakami KS. An introduction to the structure and function of the catalytic core enzyme of *Escherichia coli* RNA Polymerase. *EcoSal Plus*. 2018;8(1). <https://doi.org/10.1128/ecosalplus.ESP-0004-2018>.
123. De Las Penas A, Connolly L, Gross CA. The SigmaE-mediated response to extracytoplasmic stress in *Escherichia coli* is transduced by RseA and RseB, two negative regulators of SigmaE. *Mol Microbiol*. 1997;24(2):373–85.
124. Paget MS. Bacterial Sigma factors and Anti-Sigma factors: structure, function and distribution. *Biomolecules*. 2015;5(3):1245–65.
125. Darwin AJ. The phage-shock-protein response. *Mol Microbiol*. 2005;57(3):621–8.
126. Jones SE, Lloyd LJ, Tan KK, Buck M. Secretion defects that activate the phage shock response of *Escherichia coli*. *J Bacteriol*. 2003;185(22):6707–11.
127. Raetz CR, Guan Z, Ingram BO, Six DA, Song F, Wang X, et al. Discovery of new biosynthetic pathways: the lipid A story. *J Lipid Res*. 2009;50(SupplSuppl):S103–8.
128. Naumann A, Alesio J, Poonia M, Bothun GD. PFAS fluidize synthetic and bacterial lipid monolayers based on hydrophobicity and lipid charge. *J Environ Chem Eng*. 2022. <https://doi.org/10.1016/j.jece.2022.107351>.
129. Colin R, Ni B, Laganenka L, Sourjik V. Multiple functions of flagellar motility and chemotaxis in bacterial physiology. *FEMS Microbiol Rev*. 2021. <https://doi.org/10.1093/femsre/fuab038>.
130. Abdelwahed EK, Hussein NA, Moustafa A, Moneib NA, Aziz RK. Gene networks and pathways involved in *Escherichia coli* response to multiple stressors. *Microorganisms*. 2022. <https://doi.org/10.3390/microorganisms10091793>.
131. Laganenka L, Colin R, Sourjik V. Chemotaxis towards autoinducer 2 mediates autoaggregation in *Escherichia coli*. *Nat Commun*. 2016;7:12984.
132. González Barrios AF, Zuo R, Hashimoto Y, Yang L, Bentley WE, Wood TK. Autoinducer 2 controls biofilm formation in *Escherichia coli* through

- a novel motility quorum-sensing regulator (MqsR, B3022). *J Bacteriol.* 2006;188(1):305–16.
133. Weathers TS, Higgins CP, Sharp JO. Enhanced biofilm production by a toluene-degrading *Rhodococcus* observed after exposure to perfluoroalkyl acids. *Environ Sci Technol.* 2015;49(9):5458–66.
 134. Harbor CS. M9 minimal medium (standard). *Cold Spring Harb Protoc.* 2010;2010.
 135. team P, RStudio. Integrated development environment for R. Boston, MA: Posit Software, PBC; 2022.
 136. Team RC. R: A Language and environment for statistical computing. Vienna, Austria: R Foundation for Statistical Computing; 2022.
 137. Institute TB. Trim Galore [Available from: <https://github.com/FelixKrueger/TrimGalore>].
 138. Martin M. Cutadapt removes adapter sequences from High-Throughput sequencing reads. *EMBnetJournal.* 2021;17(1). <https://doi.org/10.14806/ej.17.1.200>.
 139. Andrews S, FastQC. A Quality Control Tool for High Throughput Sequence Data [Online]. 2010.
 140. Thakur V. RNA-seq data analysis for differential gene expression using HISAT2-StringTie-Balgon pipeline. *Methods Mol Biol.* 2024;2812:101–13.
 141. Danecek P, Bonfield JK, Liddle J, Marshall J, Ohan V, Pollard MO, et al. Twelve years of samtools and BCFtools. *Gigascience.* 2021. <https://doi.org/10.1093/gigascience/giab008>.
 142. Pertea M, Pertea GM, Antonescu CM, Chang TC, Mendell JT, Salzberg SL. Stringtie enables improved reconstruction of a transcriptome from RNA-seq reads. *Nat Biotechnol.* 2015;33(3):290–5.
 143. Sonesson C, Love MI, Robinson MD. Differential analyses for RNA-seq: transcript-level estimates improve gene-level inferences. *F1000Res.* 2015;4:1521.
 144. Kanehisa M, Goto S. KEGG: Kyoto encyclopedia of genes and genomes. *Nucleic Acids Res.* 2000;28(1):27–30.
 145. Wu T, Hu E, Xu S, Chen M, Guo P, Dai Z, et al. Clusterprofiler 4.0: a universal enrichment tool for interpreting omics data. *Innov (Camb).* 2021;2(3):100141.
 146. Karp PD, Paley S, Caspi R, Kothari A, Krummenacker M, Midford PE, et al. EcoCyc Database (2023) EcoSal Plus. 2023;11(1):eesp00022023.
 147. Edgar R, Domrachev M, Lash AE. Gene expression omnibus: NCBI gene expression and hybridization array data repository. *Nucleic Acids Res.* 2002;30(1):207–10.

Publisher's Note

Springer Nature remains neutral with regard to jurisdictional claims in published maps and institutional affiliations.